New VIV, VIVO, VVO, and VVO2Systems: Exploring their Interconversion in Solution, Protein Interactions, and Cytotoxicity

New V^{IV}, $V^{IV}O$, $V^{V}O$ and $V^{V}O_2$ Systems: Exploring their Interconversion in Solution, Protein Interactions and Cytotoxicity

Atanu Banerjee,[†] Subhashree P. Dash,[†] Monalisa Mohanty,[†] Gurunath Sahu,[†] Giuseppe Sciortino,[&,§] Eugenio Garribba,[,&] M. Fernanda N.N. Carvalho,[‡] Fernanda Marques,[‖] João Costa Pessoa,[*,‡] Werner Kaminsky,[⊥] Krzysztof Brzezinski,[¶] and Rupam Dinda[*,†]*

[†]Department of Chemistry, National Institute of Technology, Rourkela, 769008 Odisha, India

[&]Dipartimento di Chimica e Farmacia, Università di Sassari, Via Vienna 2, I-07100 Sassari, Italy

[§]Departament de Química, Universitat Autònoma de Barcelona, 08193 Cerdanyola del Vallés, Barcelona, Spain

[‡]Centro de Química Estrutural and Departamento de Engenharia Química, Instituto Superior Técnico, Universidade de Lisboa, Avenida Rovisco Pais, 1049-001 Lisboa, Portugal

[‖]Centro de Ciências e Tecnologias Nucleares, Instituto Superior Técnico, Universidade de Lisboa, Estrada Nacional 10, 2695-066 Bobadela LRS, Portugal

[⊥]Department of Chemistry, University of Washington, Box 351700, Seattle, WA 98195, USA

[¶] Faculty of Chemistry, University of Bialystok, Ciolkowskiego 1K, 15-245, Bialystok, Poland

ABSTRACT

The synthesis and characterization of one oxidoethoxidovanadium(V) [$V^{V}O(L^{1})(OEt)$] (**1**) and two non-oxidovanadium(IV) complexes, [$V^{IV}(L^{2-3})_2$] (**2** and **3**), with aroylhydrazone ligands incorporating naphthalene moieties, are reported. The synthesized oxido and non-oxido vanadium complexes are characterized by various physicochemical techniques and their molecular structures are solved by single crystal X-ray diffraction (SC-XRD). This revealed that in **1** the geometry around the vanadium atom corresponds to a distorted square pyramid, with a O_4N coordination sphere, whereas that of the two non-oxido V^{IV} complexes **2** and **3** corresponds to a distorted trigonal prismatic arrangement with a O_4N_2 coordination sphere around each "bare" vanadium center. In aqueous solution, the $V^{V}O$ moiety of **1** undergoes a change to $V^{V}O_2$ species, yielding $[V^{V}O_2(L^{1})]^{-}$ (**1'**), while the non-oxido V^{IV}-compounds **2** and **3** are partly converted into their corresponding $V^{IV}O$ complexes, [$V^{IV}O(L^{2-3})(H_2O)$] (**2'** and **3'**). Interaction of these $V^{V}O_2$, $V^{IV}O$ and V^{IV} systems with two model proteins, ubiquitin (Ub) and lysozyme (Lyz), is investigated through docking approaches, which suggest the potential binding sites: the interaction is covalent for species **2'** and **3'**, with the binding to Glu16, Glu18 and Asp21 for Ub, and His15 for Lyz, and it is non-covalent for species **1'**, **2** and **3**, with the surface residues of the proteins. The ligand precursors and complexes are also evaluated for their *in vitro* antiproliferative activity against ovarian (A2780) and prostate (PC3) human cancer cells, and in normal fibroblasts (V79) to check the selectivity of the compounds for cancer cells.

Keywords: Oxidoethoxidovanadium(V)/ Non-oxidovanadium(IV)/ Solution studies / Docking studies/ Protein interaction/ Antiproliferative activity.

INTRODUCTION

Due to the prospective application of vanadium compounds as therapeutic agents,[1–5] vanadium coordination chemistry has been an area of extensive research. For metal-based compounds to show pharmacological effects, one of the relevant aspects is their ability to interact with proteins, in order to allow their storage and/or enzymatic action in organisms.[5,6] In this context, attention has been devoted towards the study of vanadium binding to proteins, as interactions taking place with a number of peptides and proteins can regulate their transport in blood and cells, as well as cellular uptake, and is relevant for the mechanisms of action. For instance, vanadium in human blood serum is expected to be bound to human serum transferrin (hTf),[7–9] and binding to hemoglobin is also relevant once vanadium ions enter red blood cells.[10–12] In their turn, oxidovanadates(IV,V) are well known for their insulin enhancing activity, an effect that appears to be related to protein tyrosine phosphatase inhibition.[2,13–15]

However, proper understanding of the three-dimensional interactions of vanadium compounds with most relevant biomolecules, namely cellular proteins, is lacking. Single-crystal X-ray diffraction (SC-XRD) analysis and spectroscopic techniques such as nuclear magnetic resonance (NMR) for diamagnetic vanadium(V) and electron paramagnetic resonance (EPR) for vanadium(IV) compounds, as well as circular dichroism (CD) and mass spectrometry (MS) techniques have been employed to study the interactions of metal complexes with biological “receptors” at molecular level. Yet, these techniques seldom provide an explicit idea about the region of the protein where the metal is bound, as well as about the specific amino acid residues involved in the coordination. Therefore, implementation of computational methods along with the use of the above techniques is required; such approach can provide relevant information on the biological and

pharmacological roles of metal complexes by enabling the prediction of the nature of the metallodrug–protein interactions.

Molecular docking can produce fast and accurate predictions of the binding of synthesized metal complexes with various biomolecules and both relative affinities and geometries can be calculated, which are of prime importance in drug design.[16,17] Recently, docking techniques have been extended by some of us to the field of bioinorganic chemistry improving their scoring functions to evaluate the metal mediated binding.[18–22]

On the other hand, the nature of the ligand is important in the development of metal complexes and on their particular biological and reactivity characteristics; namely, the electron donor and acceptor properties, functional groups present on its backbone and their relative position in the coordination sphere are relevant aspects.[23–25] The interest in the study of hydrazone-based ligands has been increasing significantly because of the varied ligation properties due to the presence of several coordination sites,[26] as well as due to their applications in the fields of analytical[27] and medicinal chemistry.[28–31]

Over the past few years, we have been working in the field of vanadium chemistry incorporating O,N donor aroylhydrazone and azine ligands, and we have successfully isolated several oxidovanadium(V),[32–37] oxidovanadium(IV),[38–40] mixed valence oxidovanadium(IV,V)[41–43] and some rare stable non-oxidovanadium(IV) complexes,[44,45] and accessed their solution chemistry and biological activity such as protein/DNA interaction, insulin enhancing and antiproliferative activity.

Herein, we report the syntheses and characterization by several techniques, including SC-XRD, of one oxidoethoxidovanadium(V) (**1**) and two non-oxidovanadium(IV) (**2**−**3**) complexes incorporating three tridentate ONO containing aroylhydrazone ligands $(L^{1\text{-}3})^{2-}$ derived from 2-hydroxy-1-naphthaldehyde. The observed UV-Vis and EPR spectroscopic properties were further interpreted by DFT simulation studies.

Ligand-exchange and redox chemistry of vanadium in biological conditions, leading to unpredictable pharmacokinetics have hampered the introduction of V-based drugs into clinical practice.[5,15,46–49] The biological activity of several non-oxido V^{IV}-complexes has recently received attention,[15,31,44,46,50] and for example the insulin-like properties of $\{[V^{IV}(catecholato)_3]^{2-}\}$[15] and the antiproliferative activity of $[V^{IV}(dtbc)_3]^{2-}$ (dtbc = 3,5-di-*tert*-butylcatecholato)[46] were ascribed to the products of their hydrolysis/oxidation, i.e. V^{IV}- and V^{V}-oxido species. In this study, we also address the hydrolysis and redox behaviour of complexes **1-3**.

In aqueous solution, the oxidoethoxidovanadium $V^{V}O$-complex (**1**) undergoes a change to a $V^{V}O_2$ species $[V^{V}O_2(L^1)]^-$ (**1'**), while the non-oxido V^{IV}-complexes (**2** and **3**) are partly converted into their corresponding $V^{IV}O$ species, yielding $[V^{IV}O(L^2)(H_2O)]$ (**2'**) and $[V^{IV}O(L^3)(H_2O)]$ (**3'**). We evaluated the interaction of these $V^{V}O_2$, $V^{IV}O$ and V^{IV} species with two model proteins, ubiquitin (Ub) and lysozyme (Lyz), using docking approaches, which allowed predicting the most stable binding sites. The *in vitro* antiproliferative activity of complexes **1-3** and of the corresponding ligand precursors were also examined against ovarian (A2780) and prostate (PC3) human cancer cells. To check the selectivity of the compounds for cancer cells, the cytotoxic studies were also performed against normal fibroblasts (V79).

EXPERIMENTAL AND COMPUTATIONAL SECTION

General Methods and Materials. The metal precursor $[V^{IV}O(acac)_2]$ was prepared according to standard procedures described in the literature.[51] Most of the used chemicals were acquired from commercial sources and utilized without further purification; reagent grade solvents were dried and distilled prior to use as described in the literature.[52] IR spectra of the compounds were recorded using a Perkin Elmer Spectrum RXI spectrophotometer. A

Vario ELcube CHNS elemental analyzer was used for the determination of elemental analyses and PerkinElmer spectrophotometers (Lambda 25 and Lambda 35) were used to record the electronic spectra. NMR spectra (^{1}H, ^{13}C, and ^{51}V NMR) data were recorded on 400 MHz Bruker Ultrashield spectrometer utilizing $SiMe_4$ as an internal standard to measure the corresponding chemical shifts (δ_H and δ_C) in ppm. $V^{V}OCl_3$ was used as an external reference sample for ^{51}V NMR to measure the chemical shifts (δ_V), also expressed in ppm. EPR spectra were recorded in dichloromethane (DCM), in aqueous solution or in a phosphate buffer, from 0 to 8000 Gauss at liquid nitrogen temperature (77 K), with an X-band Bruker EMX spectrometer equipped with a HP 53150A microwave frequency counter. The microwave frequency was in the range 9.40-9.41 GHz, microwave power was 20 mW, time constant was 81.92 ms, modulation frequency 100 kHz, modulation amplitude 0.4 mT, resolution 4096 points. To extract the experimental spin Hamiltonian parameters, the spectra were generated with WinEPR SimFonia[53] using a linewidth for the *x*, *y* and *z* axes of 12, 12 and 7-8 Gauss and a ratio Lorentzian/Gaussian of 1.

The cyclic voltammograms of complexes **1**−**3** were obtained under N_2 from solutions of the complexes in DCM using tetrabutylammonium tetrafluoroborate (Bu_4NBF_4) 0.10 M as electrolyte. A three compartment cell provided with platinum wire electrodes (working and secondary) and a silver wire (reference) electrode interfaced with a VoltaLab PST050 equipment was used, and data were acquired by a Pentium(R) Dual-Core computer. The potentials were measured in Volt (± 10 mV) *versus* SCE at 200 mV/s using $[Fe(\eta^5\text{-}C_5H_5)_2]^{0/+}$ ($E_{1/2}^{red}$ = 0.475 V, DCM) or camphorquinone ($E_{1/2}^{red}$ = -1.34 V, DCM) as internal reference. A LCQ Fleet™ Ion Trap Mass Spectrometer from Thermo Scientific was used to measure Electrospray Ionisation Mass Spectra (ESI-MS) of aqueous/methanolic solutions of complexes **1** and **2**, in the negative- and positive-ion mode, for characterization of their

aqueous solution behavior. In the case of complex **2** a H_2O/MeOH/acetonitrile solution was also used.

Synthesis of the ligand precursors ($H_2L^{1–3}$). The aroylhydrazone Schiff base compounds, $H_2L^{1–3}$ (see **Scheme 1**), were synthesized by the condensation of 2-hydroxy-1-naphthaldehyde in ethanol with their respective acid hydrazides (for H_2L^1 = 3-hydroxy-2-naphthoic hydrazide, H_2L^2 = salicyloyl hydrazide and H_2L^3 = anthranilic acid hydrazide) in equimolar proportions.[54] The resultant yellowish compounds were filtered, washed with hot water and dried over $CaCl_2$. Elemental analysis, NMR (^1H and ^{13}C) and IR data for all compounds verified their composition. Characterization of H_2L^1 is listed below, whereas that of H_2L^{2-3} was reported earlier.[54]

H_2L^1. Yield: 71%. Anal. calcd for $C_{22}H_{16}N_2O_3$: C, 74.15; H, 4.53; N, 7.86. Found: C, 74.03; H, 4.61; N, 7.59. IR (KBr pellet, cm^{-1}): 3489 ν(O−H); 3059 ν(N−H); 1649 ν(C=O); 1599 ν(C=N). ^1H NMR (400 MHz, DMSO-d_6, ppm): δ_H 11.79 (s, 1H, naphthoyl hydrazide−OH), 11.65 (s, 1H, OH), 10.91 (s, 1H, NH), 10.03 (s, 1H, HC=N), 8.67−7.22 (m, 12H, aromatic). ^{13}C NMR (100 MHz, DMSO-d_6, ppm): δ_C 166.8, 155.8, 154.2, 153.1, 135.7, 132.8, 130.3, 129.9, 129.0, 128.1, 127.7, 127.0, 126.4, 125.1, 124.5, 124.0, 123.5, 121.6, 119.7, 118.7, 111.2, 110.4.

Synthesis of the oxidoethoxidovanadium(V) compound [$V^VO(L^1)(OEt)$] (1). The metal precursor [$V^{IV}O(acac)_2$] was added to a hot ethanolic (30 mL) solution of H_2L^1 in a stoichiometric ratio and refluxed for 3 h. The resulting brownish mixture was filtered and the filtrate was kept for crystallization by slow evaporation. After 4 days, single crystals suitable for SC-XRD structure determination were isolated from the filtrate. An outline of synthesis of this V^VO complex is depicted in **Scheme 1**.

$[V^{V}O(L^{1})(OEt)]$. Yield: 63%. Anal. calcd for $C_{24}H_{19}N_2O_5V$: C, 61.81; H, 4.11; N, 6.01. Found: C, 61.77; H, 4.08; N, 6.37. IR (KBr pellet, cm^{-1}): 3436 ν(O–H), 1597 ν(C=N), 1244 $\nu(C–O)_{enolic}$, 982 ν(V=O). UV-vis (DCM) [λ_{max}, nm (ε, M^{-1} cm^{-1})]: 445 (1966), 356 (4912), 309 (4613). ^{1}H NMR (400 MHz, DMSO-d_6, ppm): δ_H 11.23 (s, 1H, naphthoyl hydrazide−OH), 10.02 (s, 1H, HC=N), 8.67−7.19 (m, 12H, aromatic), 3.43 (m, 2H, CH_2 (OEt)), 1.06 (t, 3H, CH_3 (OEt)). ^{13}C NMR (100 MHz, DMSO-d_6, ppm): δ_C 164.6, 161.4, 154.7, 143.8, 139.5, 136.3, 135.8, 131.8, 130.5, 129.5, 129.1, 128.7, 127.2, 126.2, 125.5, 124.2, 122.9, 120.5, 119.4, 115.6,111.0, 56.5, 18.9. ^{51} V NMR (DMSO-d_6, ppm): δ_V -552.5.

Synthesis of non-oxidovanadium(IV) complexes $[V^{IV}(L^{2-3})_2]$ (2 and **3)**. Ligand precursors (H_2L^2 or H_2L^3) (2 mmol) were added to a hot CH_3CN (30 mL) solution of the metal precursor $[V^{IV}O(acac)_2]$ (1 mmol) under nitrogen atmosphere.[44] The color immediately changed to greenish black and the mixture was allowed to reflux for 3 h. Greenish black crystals of **2** were directly obtained from the reaction mixture, while a greenish black microcrystalline compound was obtained in case of **3**, which was recrystallized in CH_2Cl_2 to obtain $[V^{IV}(L^3)_2]\cdot 2CH_2Cl_2$. The crystals were then filtered off, washed thoroughly with ethanol, and dried over $CaCl_2$. **Scheme 1** depicts an outline of the steps to obtain the non-oxidovanadium(IV) complexes.

$[V^{IV}(L^2)_2]$. Yield: 73%. Anal. Calcd. for $C_{36}H_{24}N_4O_6V$: C, 65.56; H, 3.67; N, 8.49. Found: C, 65.59; H, 3.64; N, 8.44. IR (KBr pellet, cm^{-1}): 3321 ν(O–H), 1609 *ν*(C=N), 1234 $\nu(C–O)_{enolic}$. UV–Vis (DCM) [λ_{max}, nm (ε, M^{-1} cm^{-1})]: 654 (780), 544 (989), 381 (2855), 335 (3979).

$[V^{IV}(L^3)_2]\cdot 2CH_2Cl_2$. Yield: 69%. Anal. Calcd. for $C_{38}H_{30}Cl_4N_6O_4V$: C, 55.16; H, 3.65; N, 10.16. Found: C, 55.19; H, 3.72; N, 10.22. IR (KBr pellet, cm^{-1}): 1652 *ν*(C=N), 1242 ν(C–

O)$_{enolic}$. UV–Vis (DCM) [λ_{max}, nm (ε, M^{-1} cm^{-1})]: 642 (978), 546 (1384), 398 (3074), 324 (3793).

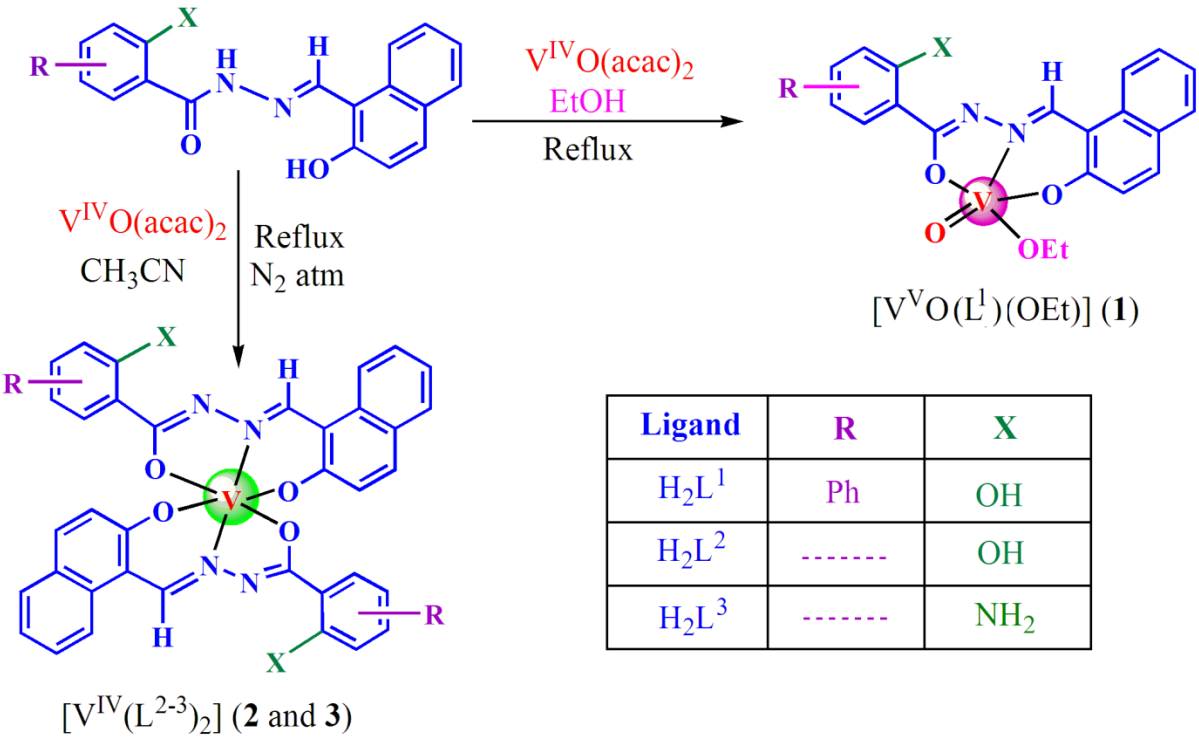

Ligand	R	X
H_2L^1	Ph	OH
H_2L^2	-------	OH
H_2L^3	-------	NH_2

Scheme 1. Schematic representation of the synthesis of $[V^{V}O(L^{1})(OEt)]$ (**1**) and $[V^{IV}(L^{2-3})_2]$ (**2** and **3**) compounds.

X-ray Crystallography

A red needle shaped prism of **1** (size: 0.60×0.02×0.01 mm^3), and black prisms of **2** (0.22×0.19×0.07 mm^3) and **3** (0.25×0.21×0.12 mm^3) were each mounted on a loop with oil. The X-ray diffraction data of **1** and **3** were collected at 19 °C on a Bruker APEX II single crystal X-ray diffractometer and at -143 °C on Nonius Kappa CCD FR590 single crystal X-ray diffractometer, respectively, using Mo K_α radiation. Diffraction data of **2** were collected at -173 °C on a SuperNova diffractometer (Rigaku) with a CCD detector and $Cu_{K\alpha}$ radiation. The data of **1** was integrated and scaled using SAINT, SADABS within the APEX2 software package by Bruker,[55] and the data of **3** was integrated and scaled using hkl-SCALEPACK.[56]

This program applies a multiplicative correction factor (S) to the observed intensities (I) and has the following form: $S = (e^{-2B(\sin^2\theta)/\lambda^2})/\text{scale}$, where S is calculated from the scale and the *B* factor determined for each frame and is then applied to I to give the corrected intensity (I_{corr}).

The structures of **1**−**3** were solved by direct methods (SHELXS, SIR97[57] SHELXT[58]) to produce complete heavy atom phasing model consistent with the proposed structures and then completed by difference Fourier synthesis with SHELXL97[59] and SHELXL.[60] Indexing and unit cell refinement indicated that complex **1** crystallizes in orthorhombic space group P n a 2_1, complex **2** in monoclinic space group *C* 2/c, and complex **3** in triclinic space group $P\bar{1}$. **Table S1** contains all the crystallographic data as well as structure solution and refinement details of **1**−**3**. The observed data / R(int) = 5139, 0.0969 (**1**), 3152, 0.041 (**2**) and 8583, 0.1204 (**3**) statistics indicate that the data were appropriate. Structure refinements were carried out on F^2, applying Scattering factors from Waasmaier and Kirfel.[61] All hydrogen atoms were placed in geometrically idealized positions and constrained to ride on their parent atoms with C···H distances in the range 0.95-1.00 Å. Isotropic thermal parameters Ueq were fixed such that they were 1.2Ueq of their parent atom Ueq for CH's, and 1.5Ueq of their parent atom Ueq in case of methyl groups. Hydroxyl hydrogen atoms were freely refined without any constraints or restraints. All non-hydrogen atoms were refined anisotropically by full-matrix least-squares. Disordered solvent within a void of 76 $Å^3$ in **2** required to use the solvent mask procedure implemented in OLEX2.[62] Crystallographic data integrity was validated with PLATON.[63] CCDC numbers 1976254 (**1**), 1961784 (**2**), and 1976255 (**3**) contain the supplementary crystallographic data for these compounds. These data can be obtained free of charge from the Cambridge Crystallographic Data Centre via www.ccdc.cam.ac.uk/data_request/cif.

Computational studies

The geometry of V complexes was optimized and harmonic frequencies were computed with Gaussian 09 software[64] at DFT theory level, combining the B3P86 functional[65,66] with the Pople basis set 6-311g. This method has been successfully applied and discussed in the literature for the geometry prediction of vanadium complexes.[67,68] DFT stability calculations in solution have been carried out with the SMD continuum model[69] for water and including diffuse and polarization functions (basis set 6-311++g(d,p)) for all atoms. The ^{51}V hyperfine coupling tensor $\boldsymbol{A}$ was calculated with ORCA software[70] on the optimized structures with the double hybrid functional B2PLYP[71] and the basis set VTZ. The ^{51}V HFC tensor $\boldsymbol{A}$ was calculated from the contributions of the isotropic Fermi contact (A^{FC}), dipolar hyperfine interaction ($\boldsymbol{A}^{D}$) and spin-orbit (SO) term ($\boldsymbol{A}^{SO}$).[72,73] The percent deviation (PD) of the absolute calculated value, $|A_z|^{calcd}$, from the absolute experimental value, $|A_z|^{exptl}$, was obtained as follows: $100 \times [(|A_z|^{calcd} - |A_z|^{exptl})/|A_z|^{exptl}]$.

Time-dependent density functional theory (TD-DFT) calculations[74] were used to predict the excited-states and electronic absorption spectrum of the non-oxido complex **3**. The simulations were carried out on the geometry optimized in the gas phase using CAM-B3LYP functional and 6-31+g(d) basis set, according to the method established previously.[45,75] The predicted electronic spectrum of **3** was generated using Gabedit software.[76]

The docking calculations were performed with GOLD 5.8 software[77] according to the procedures recently reported[18,20–22,78–80] to study the possible binding to ubiquitin and lysozyme of all the enantiomers (both clockwise and anticlockwise enantiomers were considered) of non-oxido complexes **2** and **3** and oxidovanadium species $[V^{V}O_2(L^{1})]^-$ (**1'**) derived from **1**, and $[V^{IV}O(L^{2\text{-}3})(H_2O)]$ (**2'** and **3'**) derived from **2-3**. $[V^{V}O_2(L^{1})]^-$ (**1'**) and $[V^{IV}(L^{2\text{-}3})_2]$ (**2**, **3**) could bind to Ub and Lyz only through second coordination sphere

interactions (non-covalent binding), while for oxidovanadium(IV) fragments **2'** and **3'** the binding may occur in an accessible equatorial position upon the replacement of monodentate H_2O ligand (covalent binding). With the aim to individuate the most exposed potential coordinating residues, the relative Solvent Excluded Surface (SES) of Ub and Lyz was computed.[81] Docking calculations were carried out building an evaluation sphere of 12 Å containing the potential amino acid donors identified by SES analysis. Surface dockings in the systems with non-covalent interactions between **1'**, **2** and **3** and Ub and Lyz were performed considering the whole rigid protein, while for the docking simulations with covalent bonds vanadium–protein (**2'** and **3'**), the side chains flexibility was taken into account using the rotamers libraries implemented in GOLD.[82] Genetic algorithm (GA) parameters have been set in 50 GA runs and a minimum of 100,000 operations. The other parameters of GA were set to default. The scoring (*Fitness* of GoldScore) was evaluated through the recent validated versions of GoldScore accounting for coordination bonds and surface interactions.[25] The best solutions (binding poses) were evaluated taking into account the mean (F_{mean}) and the highest value (F_{max}) of the scoring and population of the cluster containing the best pose.

Determination of cytotoxic activity

The cytotoxicity of the ligand precursors and their corresponding vanadium complexes was evaluated in ovarian (A2780) and prostate (PC3) cancer cells and in normal fibroblasts (V79). All cell lines were grown in RPMI medium supplemented with 10% FBS and maintained at 37 ºC in an incubator (Heraeus, Germany) with 5% CO_2 and humidified atmosphere. MTT assay was used to assess the cellular viability.[37,83] For the assays, cells were seeded in 96-well plates, at a density of 1-2×10^4 cells/200 µL medium, and allowed to adhere overnight. Ligand and complexes were first diluted in DMSO and then in culture medium to prepare a series of

dilutions in the range of 10^{-7}–10^{-4} M. The maximum concentration of DMSO in the medium was 1% and, at this percentage, no cytotoxic effect was observed due to DMSO. After incubation for 48 h with the compounds, the medium was discarded and 200 μL of MTT solution in PBS (0.5 mg/mL) were added to each well. After 3 h at 37 °C, the medium was removed and replaced by 200 μL DMSO to solubilise the formazan crystals. The cellular viability (% control) was assessed by measuring the absorbance at 570 nm using a plate spectrophotometer (Power Wave Xs, Bio-Tek). The IC_{50} values were calculated using the GraphPad Prism software (version 5.0). Results are shown as the mean ± SD of at least two independent experiments done with six replicates each.

RESULTS AND DISCUSSION

Synthesis

Scheme 1 outlines the synthesis of monomeric oxidoethoxidovanadium(V) ($V^{V}O$) (**1**) and non-oxidovanadium(IV) (V^{IV}) (**2** and **3**) complexes. Complex **1** was synthesized by refluxing the metal precursor $[V^{IV}O(acac)_2]$ in a hot ethanolic solution of aroylhydrazone H_2L^1 in stoichiometric amounts (1:1 mol ratio). Under reflux conditions, V^{IV} was oxidized by the aerial oxygen and an ethoxido coordinated vanadium(V) complex was isolated as final product.

In contrast, the reaction of $[V^{IV}O(acac)_2]$ with H_2L^{2-3} in CH_3CN medium under N_2 atmosphere in 1:2 mol ratio led to the formation of the non-oxidovanadium $[V^{IV}(L^{2-3})_2]$ (compounds **2**–**3**). This reaction can be represented by equation (1).

$$2\ H_2L^{2\text{-}3} + [V^{IV}O(acac)_2] \rightarrow [V^{IV}(L^{2\text{-}3})_2] + 2Hacac + H_2O \quad (1)$$

IR Spectroscopy

Most of the IR spectral information is summarized in the Experimental Section. The ligands (H_2L^{1-3}) show a band in the range 3489−3320 cm^{-1} due to the aromatic −OH stretching frequency present in the naphthalene moiety, which is absent in their corresponding complexes because of deprotonation upon coordination. However, **1** and **2** possess a band in the range 3436-3321 cm^{-1}, for the uncoordinated −OH group attached to the aroylhydrazide moiety of their corresponding ligands.[36,40] The free ligands also exhibit characteristic stretching bands in the region 3059-3022 (ν_{N-H}) and 1649-1637 ($\nu_{C=O}$) cm^{-1} for their amide moiety, which are not observed in the spectra of their respective complexes (**1**–**3**). Additionally, the appearance of a new bands in the complex within 1244-1234 cm^{-1}, due to the stretching vibration of the conjugated C=N–N=C–O^- moiety, clearly indicate the coordination of the ligands in their deprotonated enolic form.[45,84–87] Moreover, the presence of one sharp band at 982 cm^{-1} for **1**, due to the ν(V=O) stretching, indicates the mono-oxido nature of the complex,[33,34,43,88] while its absence in the spectra of **2** and **3** agrees with the presence of "bare" vanadium centers.[44,45,75]

Description of the molecular structures of 1–3

Detailed information on the stereochemistry of the complexes, in particular the coordination mode of the ligands, and confirmation of the non-oxido nature of compounds **2** and **3** was gathered through single-crystal X-ray diffraction experiments, which allowed to obtain the molecular structures of $[V^{V}O(L^{1})(OEt)]$ (**1**), $[V^{IV}(L^{2})_2]$ (**2**) and $[V^{IV}(L^{3})_2]\cdot 2CH_2Cl_2$ (**3**). **Figure 1** shows the molecular structures of one of the molecules of each asymmetric unit of complexes **1–3**, and selected bond distances and angles are collected in **Table S2A**.

Complex **1** (**Figure 1a**) corresponds to discrete units of monomeric $V^{V}O(OEt)$-species having a $V^{V}O^{3+}$ moiety, where the V^{V}-center is in a five-coordinated distorted square

pyramidal $V^{V}O_4N$ geometry. The basal plane is made up of the naphtholate oxygen (O1), imine nitrogen (N1), enolic oxygen (O2) of the tridentate binegative ONO-donor aroylhydrazone ligand (L^1), and the oxygen (O5) from an alkoxide, which came from the ethanol used as solvent. The remaining apical position of the square pyramid is occupied by the oxido ligand (O4). This structure also revealed different V−O bond lengths in the following order: V1−O4 of the oxido moiety (1.570(2) A°) < V−O5 of EtO^- (1.748(2) A°) < V−O1 of naphtholate (1.843(2) A°) < V−O2 of enolate (1.930(19) A°), as usually observed in such oxidoalkoxidovanadium complexes.[36,43,45,89] There is a small disorder in the EtO^- ligand; the crystal packing diagrams show that the pending hydroxyl O3 atom, attached with the naphthalene moiety of hydrazide from a neighboring molecule, interacts weakly with the vanadium, as depicted in **Figure S1**.

The molecular structures of $[V^{IV}(L^2)_2]$ (**2**) and $[V^{IV}(L^3)_2]\cdot 2CH_2Cl_2$ (**3**) are similar, (**Figure 1b-c),** and some selected geometric parameters are given in **Table S2A**. The molecular structures contain a V^{IV}-center coordinated by a pair of doubly deprotonated tridentate ONO-donor aroylhydrazones. Each of the ligands bind the V-atom *via* the naphtholate-O, imine-N and enolic-O atoms of the tridentate binegative ONO-donor aroylhydrazones. In summary, the vanadium atoms comprise trigonal prismatic $V\text{-}N_2O_4$ coordination geometries where each of the hydrazone ligands is forming a five-membered CN_2OV and a six-membered C_3NOV chelate ring. Within the crystal lattice of molecule **2** (**Figure 1b**), asymmetric unit contains half of the mononuclear non-oxidovanadium(IV) complex. The vanadium cation is located on a special position, namely crystallographic two-fold axis which generates the complete mononuclear complex molecule. However, such type of symmetry is not observed in case of **3**. Additionally, there are two dichloromethane solvent molecules of crystallization present in the crystal lattice of **3**, as shown in **Figure 1c**.

The observed V−O and V−N bond lengths around the central vanadium atom and angles for **2** and **3** are within the expected range as reported earlier in the literature.[44,45]

The crystal structure of non-oxidovanadium(IV) complexes (**2** and **3**) revealed a near perfect trigonal prismatic coordination geometry of the vanadium. The two opposing triangular faces (consisting of O1, O2 and N1 and their symmetry related ones) are rotated off each other by about 2.17(4)º (for complex **2**) and 6.70(7)º (for complex **3**), but this is within the margins by which the triangular angles deviate from 60º [(63.04º, 57.95º, and 59.01º) (**2**) and (61.07/62.38°, 58.39/58.02° and 60.54/59.60° (**3**)]. The corner lengths of the trigonal prism deviate from each other by ca. 0.13 Å for both the complexes (**2** and **3**). The corresponding geometrical parameters are also listed in **Table S2B**.

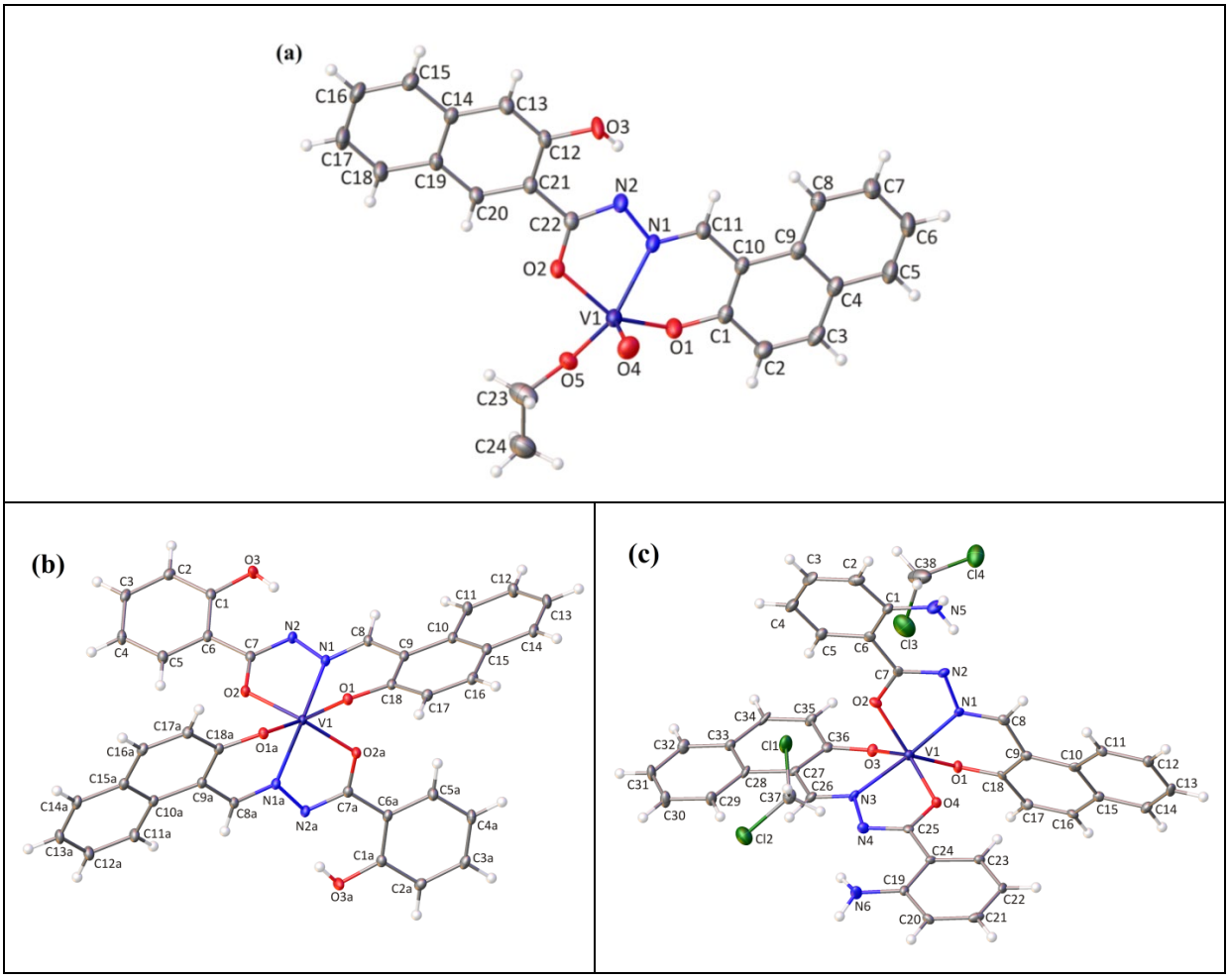

Figure 1. Molecular structures of (a) $[V^{V}O(L^{1})(OEt)]$ (**1**), (b) $[V^{IV}(L^{2})_2]$ (**2**) and (c) $[V^{IV}(L^{3})_2]\cdot 2CH_2Cl_2$ (**3**), drawn with thermal ellipsoids at the 50% probability level.

ESI Mass Spectrometry

Electrospray Ionisation Mass Spectra (ESI-MS**)** of water:methanol (ca. 90:10) solutions of complex **1** were recorded, in the negative- and positive-ion mode, for characterization of their aqueous solutions; the corresponding ESI-MS spectra are depicted in **Figures S2-S3** and **Tables S3-S4**.

From the ESI-MS spectra recorded in the negative-ion mode it is clear that upon dissolving **1**, the complex is converted to a $V^{V}O_2(L)$-type complex (peak at m/z = 437.34, 100%). Thus the process occurring is:

$$[V^{V}O(L^{1})(OEt)] + 2H_2O \rightarrow [V^{V}O_2(L^{1})]^- + EtOH + H_3O^+ \quad (2)$$

In principle, the $[V^{V}O_2(L^{1})]^-$ species formed can be 5- or 6-coordinated with an additional water molecule bound to vanadium; in fact, a monodentate solvent molecule could have been removed from the first metal coordination sphere during the ionization process.[78,90,91] To consider this possibility, the relative stability of $[V^{V}O_2(L^{1})]^-$ and $[V^{V}O_2(L^{1})(H_2O)]^-$ was calculated by DFT methods modeling the solvent effects with SMD.[69] The results indicated that for $[V^{V}O_2(L^{1})(H_2O)]^-$ an energy minimum could not be found; the H_2O ligand leaves spontaneously the axial site, suggesting that the 6-coordinated species is not stable at all in aqueous solution. Globally, these experiments indicate that when measuring the cytotoxicity of complex **1**, once this compound is added to the incubation media, it will be converted to a dioxidovanadium(V) compound $[V^{V}O_2(L^{1})]^-$.

Similarly, the ESI-MS spectra of the non-oxidovanadium compound **2** were recorded upon dissolving it in water:methanol (ca. 90:10) solutions (**Figures S4-S7** and **Tables S5-S6**). In the ESI-MS (+) experiments in water:methanol (ca. 90:10) solutions, complex **2** hardly dissolved and only gave a peak at m/z = 157.0 (100%) probably due to the fragmented ligand. Upon addition of acetonitrile to this solution, a clear peak at m/z = 660.22 (100%) showed up, corresponding to $[V^{IV}(L^{2})_2]+H^+$, as well as others: at m/z = 700.71 (~5%,

$[V^{IV}(L^2)_2]\cdot CH_3CN+H^+$), at m/z = 403.10 (~12%, $[V^{V}O(L^2)(MeOH)]^+$ or $[V^{IV}O(HL^2)(MeOH)]^+$, see SI section) and m/z = 412.81 (~20%, $[V^{IV}O(L^2)(H_2O)]+Na^+$). When doing the "washing" procedures of the MS instrument with MeOH, a clear peak at m/z = 659.40 (100%, ESI-MS(-)) showed up, apparently indicating that complex **2** is stable enough in water:MeOH solvent for several hours, so that this non-oxido V^{IV} complex can be detected by ESI-MS. Thus, from the ESI-MS data it is clear that $[V^{IV}(L^2)_2]$ is fairly stable in contact with aerated H_2O/MeOH solvents, but that significant amounts of $V^{IV}O(L^2)$-type complexes also form in these solutions. We did not manage to detect V^{V}-L^2 species by ^{51}V NMR, which might be due to the presence of high amounts of paramagnetic V^{IV}-complexes, but a minor peak was detected by ESI-MS(+) (see above and Figure S6 and Table S5), that might be due to a V^{V}-species (m/z = 403.10, ~12%, $[V^{V}O(L^2)(MeOH)]^+$); therefore it is plausible that some amount of V^{V}-species are also formed in the conditions prevailing in cell media.

UV−Vis Spectroscopy

The electronic spectra of **1**−**3** were recorded in DCM by employing concentrations in the range $1\text{-}2\times10^{-4}$ M. The $V^{V}O(OEt)$-complex (**1**) exhibits two absorptions in the range of 445-356 nm, that are attributed to ligand-to-metal charge transfer (LMCT) transitions.[33–35] The other strong absorption bands observed at higher energies, below 350 nm, may be considered as ligand centered transitions (**Figure S8a**).[34,35,45] The two non-oxidovanadium (V^{IV}) complexes (**2** and **3**) possess similar spectral features and the spectrum of **2** is depicted in **Figure S8b**. For **2** and **3**, the main bands in the visible region are LMCT, as supported by TD-DFT (see **Table 1**), while the strong absorptions at higher energy (380−320 nm) are composite bands due to LMCT and ligand centered transitions.

In order to get additional information on the nature and intensity of the transitions of the non-oxidovanadium complexes, the electronic absorption spectrum of **3** was simulated by TD-DFT methods following the protocol recently used for other 'bare' V^{IV} complexes (**Figure S9**).[45,75] The absorption wavelength and oscillator strength for the most important transitions are listed in **Table 1**. The dominant character of the transitions involves excitations from ligand centered MOs to V-*d* based MOs, mainly V-d_{yz}, V-$d_{x^2-y^2}$, and V-d_{z^2} (LMCT); however, a not negligible percent amount of ligand centered absorptions is expected. The involvement of the V-*d* orbitals in non-oxidovanadium(IV) complexes was ascertained in other studies.[92,93] Interestingly, metal-to-ligand charge transfers (MLCT) – predicted in other systems[45,92] – are not important for **3** and do not contribute significantly to the experimental absorptions. These data confirm that, for non-oxido V^{IV} complexes, most of the observable electronic transitions derive from LMCT transitions.[94]

Table 1. Calculated and experimental electronic transitions for complex **3** up to 250 nm.[a]

Transition (MO character)[b]	% V in MO	% transition	λ [c]	$f \times 10^5$ [d]	λ^{exptl} (ε^{exptl})[c,e]
H^{α}-8 → L^{α}+2 (d_{yz})	L (0% V) → M (42% V)	61.6	887.9	20	885 (127)
H^{α} → L^{α} ($d_{x^2-y^2}$)	L (0% V) → M (32% V)	23.3	593.5	430	642 (978)
H^{α}-1 → L^{α} ($d_{x^2-y^2}$)	L (4% V) → M (32% V)	17.9	507.9	370	546 (1384)
H^{α} → L^{α} ($d_{x^2-y^2}$)	L (0% V) → M (32% V)	22.3	502.6	7860	
H^{β} → L^{β} (d_{z^2})	L (0% V) → M (12% V)	14.1	441.1	6320	435 (2312)[f]
H^{β} → L^{β} (d_{z^2})	L (0% V) → M (12% V)	16.9	393.0	28310	398 (3074)
H^{β}-1 → L^{β} (d_{z^2})	L (1% V) → M (12% V)	19.6	388.7	12140	
H^{α}-1 → L^{α} ($d_{x^2-y^2}$)	L (4% V) → M (32% V)	26.4	349.8	13290	324 (3793)
H^{α}-1 → L^{α}+2 (d_{yz})	L (4% V) → M (42% V)	12.5	295.7	18060	

[a] Calculations carried out at the level of theory CAM-B3LYP/6-31+g(d). [b] H stands for HOMO and L for LUMO, and α and β indicate the electron spin. [c] λ values measured in nm. [d] Oscillator strength. [e] ε values measured in M^{-1} cm^{-1}. [f] Shoulder of a more intense absorption.

NMR Spectroscopy

^{1}H and ^{13}C NMR of all ligand precursors H_2L^{1-3} and complex **1** were recorded in DMSO-d_6. The spectra of H_2L^{1-3} exhibit two prominent characteristic singlet resonances in the range δ = 11.65−10.91 ppm due to the presence of –OH and −NH protons, respectively. The absence of these peaks in the spectrum of complex **1** indicates the deprotonation of the –OH and −NH moieties upon complexation; its ^{1}H NMR spectrum is depicted in **Figure S10**. All the aromatic protons of **1** are observed in the expected region, δ = 8.67−7.19 ppm. Furthermore, the appearance of two peaks at δ = 3.43 ppm and 1.06 ppm are attributed to the $–CH_2$ and $−CH_3$ protons, respectively, of the coordinated ethoxido ligand.[43]

The ^{13}C NMR spectrum of complex **1**, shown in **Figure S11**, contains two signals for the (CO=N) and (N=CH) carbons in the extreme downfield region at δ = 164.6 and 161.4 ppm, respectively, whereas the aromatic carbons appear in the expected region between 154.7−111.0 ppm. Two resonances for the aliphatic carbons of the EtO^- ligand are found in the upfield region at δ = 56.5 ($–CH_2$) and 18.9 ($−CH_3$) ppm.[36,43]

The ^{51}V NMR spectra of **1** displays a singlet at δ_V = −552.5 ppm in DMSO (**Figure S12**), as well in DCM (at δ_V = −565 ppm). These chemical shifts are in the range of those obtained for other mononuclear oxidoethoxidovanadium(V) complexes,[33,35,43,45,95,96] with $(L^1)^{2-}$ depicting significantly higher shielding effect.

Upon dissolving complex **2** in DMSO and adding water up to ca. 90% v/v, setting the pH in the range 4.5–7.5 and leaving the solutions standing for several hours, no ^{51}V NMR resonance was detected, except at pH 7.5, where a weak peak at δ_V = −559 ppm was observed, probably due to free vanadate.

Electrochemical properties

Complex **1** in DCM displays one anodic quasi-reversible process attributed to V(V)→V(IV) reduction (wave **I**, **Figure 2**) at $E_{1/2}^{red}$ = 0.49 V, which fits well in the range of potential reported for oxidovanadium(V) complexes with ONO type ligands.[33,35–37,42,43,45,97] Two additional irreversible cathodic waves (**II**, E_p^{red} = -0.99 V, and **III**, E_p^{red} = -1.57 V, **Figure 2**) and one lower potential reversible wave (**IV**, $E_{1/2}^{red}$ = -1.74 V, **Figure 2**) are also observed. The potential of the irreversible wave **III** is close to that of the free ligand (E_p^{red} = -1.68 V, **Figure S13**), suggesting a ligand based process; while the remaining two observed cathodic waves (**II** and **IV**) we could not able to assigned.

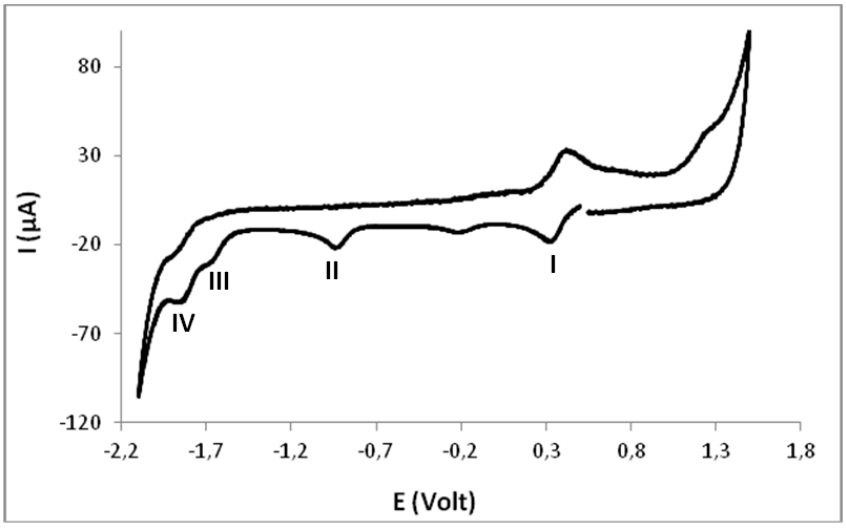

Figure 2. Cyclic voltammogram of complex **1** (E values *vs*. SCE) measured in DCM at 200 mV/s using a Pt wire electrode.

Non-oxidovanadium(IV) complexes **2** and **3** display similar electrochemical behavior in dichloromethane. Both show *quasi*-reversible cathodic processes at close potentials (wave **I**, **Figure 3** and **4**), which are attributed to V(IV)→V(III) reduction.

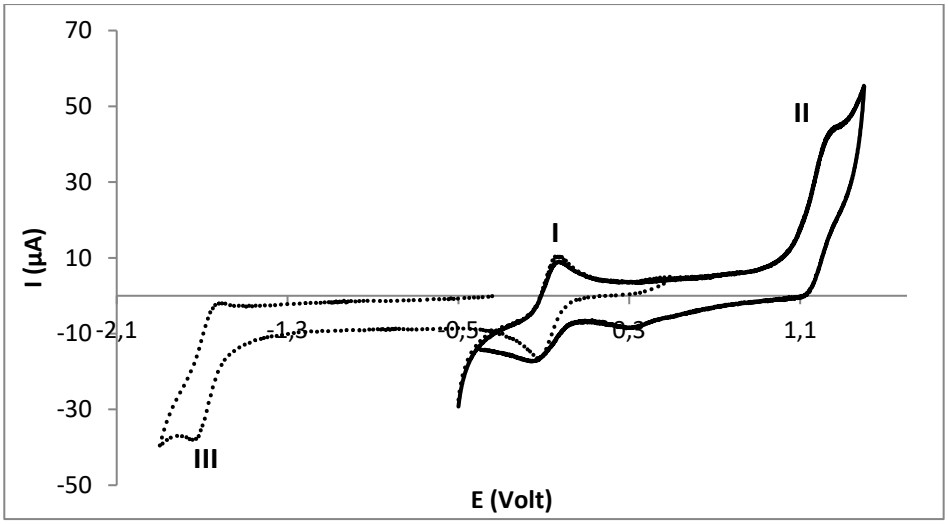

Figure 3. Cyclic voltammograms (E values *vs*. SCE) of complex **2**. Anodic scan (—) and anodic scan reversed to the cathodic region upon wave **I** (···). Data obtained in DCM at 200 mV/s, using a Pt wire electrode.

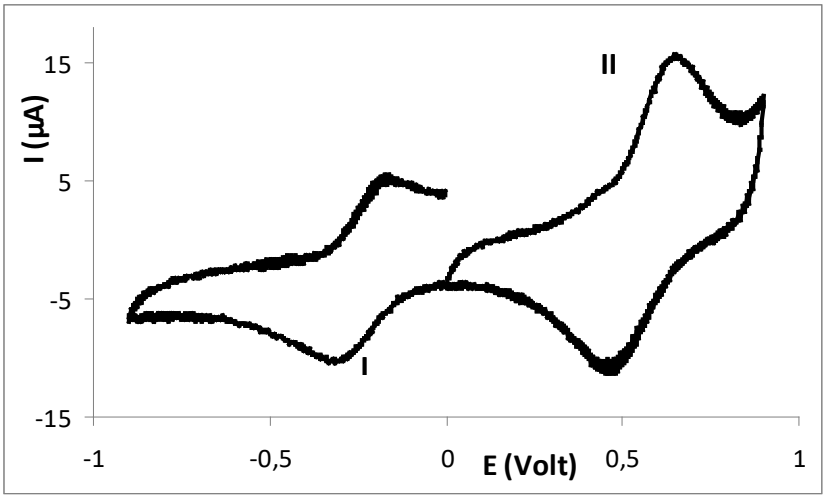

Figure 4. Cyclic voltammogram (E values vs. SCE) of complex **3** measured in DCM at 200 mV/s, using a Pt wire electrode.

Complex **2** reduces at $E_{1/2}^{red}$ = -0.012 V (**Figure 3**, wave **I**), and complex **3** at a slightly lower potential ($E_{1/2}^{red}$ = -0.18 V) (**Figure 4**, wave **I**) and both values are well in the range of

potentials observed for V(IV) non-oxido complexes.[44,45,75] Additionally, **2** displays a reversible cathodic wave at a much lower potential ($E_{1/2}^{red}$ = -1.62 V; wave **III**, **Figure 3**) which is attributed to a ligand based process. No related process was detected for complex **3**. Both complexes **2** and **3** display quasi-reversible anodic waves attributed to the V(IV)→V(V) oxidation. However, the potential of the anodic processes display considerably different values at the two complexes, *i.e*. complex **3** oxidizes at a considerably lower potential ($E_{1/2}^{ox}$ = 0.61 V) than complex **2** ($E_{1/2}^{ox}$ = 1.20 V). The relatively low oxidation potential measured for complex **3** (0.61 V) was unexpected for a neutral V^{IV} complex, since values in that range have been reported for the V(IV)→V(V) oxidation of the anionic complexes.[44,97] However, the considerably low Hammett σ parameter for the -NH_2 substituent (-0.66) at the aromatic ring evidences its high electron releasing effect (considerably higher than for the -OH substituent, -0.37), thus a higher electron density exists at the V^{IV} site,[98] this enabling a relatively low V(IV)→V(V) potential which tends to those observed in anionic complexes.

EPR spectroscopy

The anisotropic EPR spectra of the non-oxido complexes **2** and **3** were recorded in DCM at liquid nitrogen temperature (77 K). The spin Hamiltonian parameters (***g*** and ***A*** tensors) were extracted generating the experimental spectra with WinEPR software[53] and are reported in **Table 2**. The experimental and generated spectra of **2** are depicted in **Figure 5**.

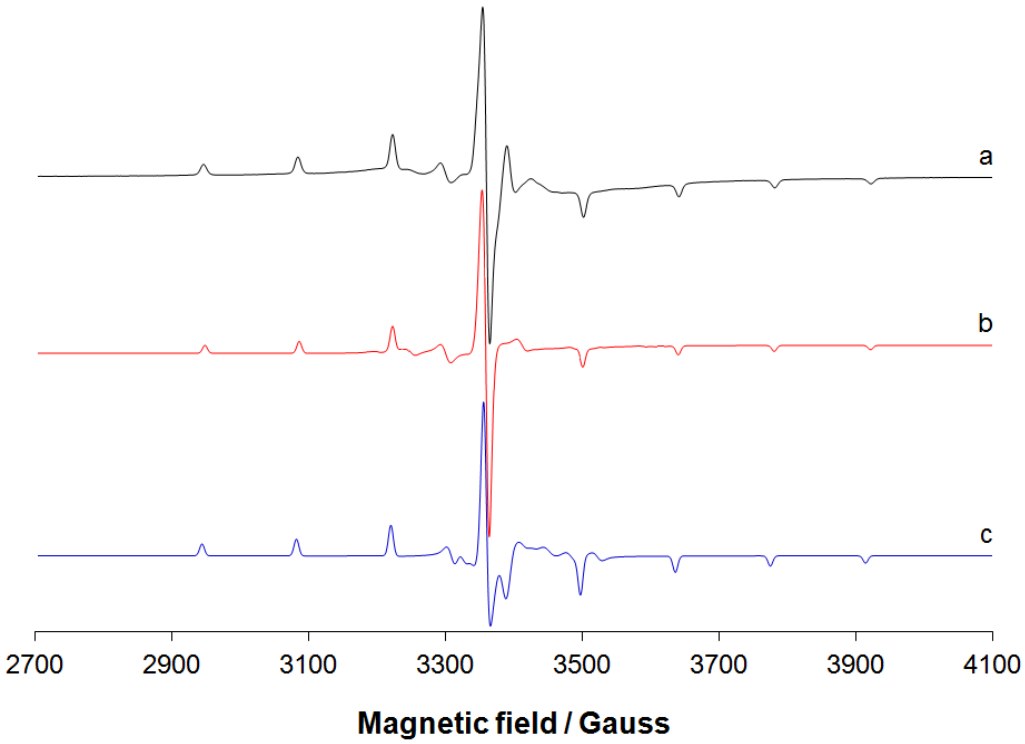

Figure 5. First derivative X-band anisotropic EPR spectra of $[V^{IV}(L^2)_2]$ (**2**): (a) experimental in DCM at 77 K, (b) generated by WinEPR software to extract the spin Hamiltonian parameters and (c) calculated by DFT methods.

Table 2. Experimental and DFT calculated spin Hamiltonian parameters (g and A values) complexes **2** and **3** in DCM.[a]

	Complex **2**		Complex **3**	
Parameter	Experimental	DFT calculated [b]	Experimental	DFT calculated [b]
g_x	1.986	1.980	1.986	1.981
g_y	1.975	1.959	1.974	1.961
g_z	1.958	1.957	1.957	1.957
A_x	-12.0	-18.2	-12.0	-18.3
A_y	-50.0	-27.9	-53.0	-27.6
A_z	-126.2	-125.7	-127.1	-126.6
PD (A_z)	-0.4		-0.4	

[a] Values of A reported in 10^{-4} cm^{-1} units. [b] Values calculated with B2PLYP functional and VTZ basis set on the optimized structures (see "Experimental and Computational" section).

The $\boldsymbol{g}$ and ^{51}V $\boldsymbol{A}$ tensors for **2** and **3** were calculated by DFT simulations with the double hybrid B2PLYP functional and VTZ basis set on the optimized structures. ORCA software was used since it includes the SO contribution, which is fundamental to correctly predict the values of $\boldsymbol{A}$, in particular the largest value of the diagonilized tensor $\boldsymbol{A}$ (A_x or A_z). This computational protocol allows calculating A_z with a percentage deviation below 4%.[73] For **2** and **3**, both the values of percent deviation (PD), defined in the "Experimental and Computational" section, for A_z are -0.4%. The contribution of second-order SO term is 6.9% for both the species and obviously cannot be neglected. The spectrum generated using the DFT data is shown in trace (c) of **Figure 5**.

In a series of studies,[73,99,100] some of us demonstrated that EPR spectra of non-oxido V^{IV}-complexes can be grouped in three different types depending on the angle Ω formed by the two external donors of the tridentate ligand: **type 1** spectra for species with geometry close to the octahedron and $|A_z|$ in the range (135-155)×10^{-4} cm^{-1}; **type 2** spectra for complexes with geometry close to the trigonal prism and $|A_x| \sim |A_y|$ in the range (90-120)×10^{-4} cm^{-1}; **type 3** for compounds with an intermediate geometry and intermediate values of $|A_x|$ or $|A_z|$, in the range (120-135)×10^{-4} cm^{-1}. In **Figure 6** the data of the complexes **2** and **3** were added to those found for other hexa-coordinated 'bare' V^{IV}-complexes;[45,75,92,99–102] it emerges that the spectra of **2** and **3** belongs to the **type 3** group, corresponding to the open-chain tridentate ligands, for which a singly occupied molecular orbital (SOMO) based on V-d_{xy} is expected.[73] This suggests that the geometry in the solid state, intermediate between the octahedral and the trigonal prismatic, is retained by compounds **2** and **3** in DCM solution.

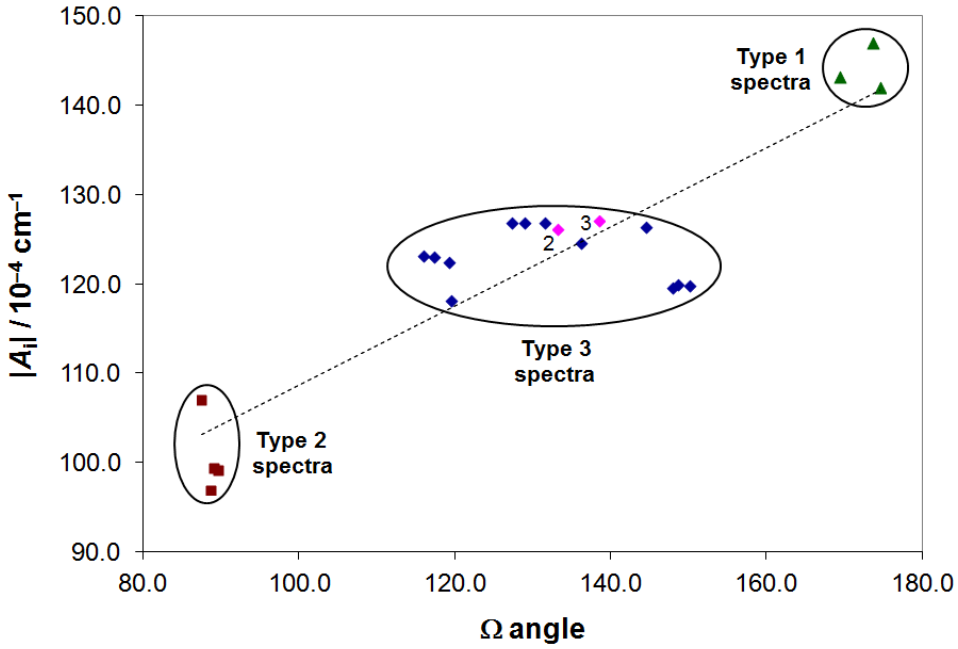

Figure 6. Experimental $|A_i|$ values for non-oxido V^{IV}-complexes as a function of the experimental Ω angles. The regions corresponding to the **type 1** (rigid ligands, green triangles), **type 2** (cyclic ligands, brown squares) and **type 3** spectra (open-chain non rigid ligands, blue rhombi). The pink rhombi in the **type 3** spectra region denote complexes **2** and **3** of this study. $|A_i|$ (i = *x* or *z*) are the largest values of the ^{51}V ***A*** tensor. The dotted line represents the best linear fitting for the twenty-one points considered.

When **2** and **3** were dissolved in water or in phosphate buffer (see the EPR spectra in **Figure 7**), the transformation to an oxidovanadium(IV) partly occurs according to the reaction (3), as substantiated by ESI-MS measurements:

$$[V^{IV}(L^{2\text{-}3})_2] + 2H_2O \rightleftarrows [V^{IV}O(L^{2\text{-}3})(H_2O)] + H_2L^{2\text{-}3} \quad (3)$$

The species $[V^{IV}O(L^2)(H_2O)]$ and $[V^{IV}O(L^3)(H_2O)]$ are abbreviated as **2'** and **3'**. The g_z and $|A_z|$ for $[V^{IV}O(L^2)(H_2O)]$ are 1.949 and 164.5×10^{-4} cm^{-1} (H_2O, pH 5) and 1.948 and 164.9×10^{-4} cm^{-1} (phosphate buffer); for $[V^{IV}O(L^3)(H_2O)]$ they are 1.948 and 164.4×10^{-4} cm^{-1} (H_2O, pH 5) and 1.948 and 164.7×10^{-4} cm^{-1} (phosphate buffer). The bianionic ligands $(L^2)^{2-}$

and $(L^3)^{2-}$ bind $V^{IV}O^{2+}$ in a tridentate fashion with the (O^-, N, O^-) donors on the equatorial plane, the remaining position being occupied probably by a solvent molecule. The spin Hamiltonian parameters are comparable to those measured for other 1:1 $V^{IV}O$ species formed by tridentate ligands with a similar coordination mode.[40,99,100,103,104]

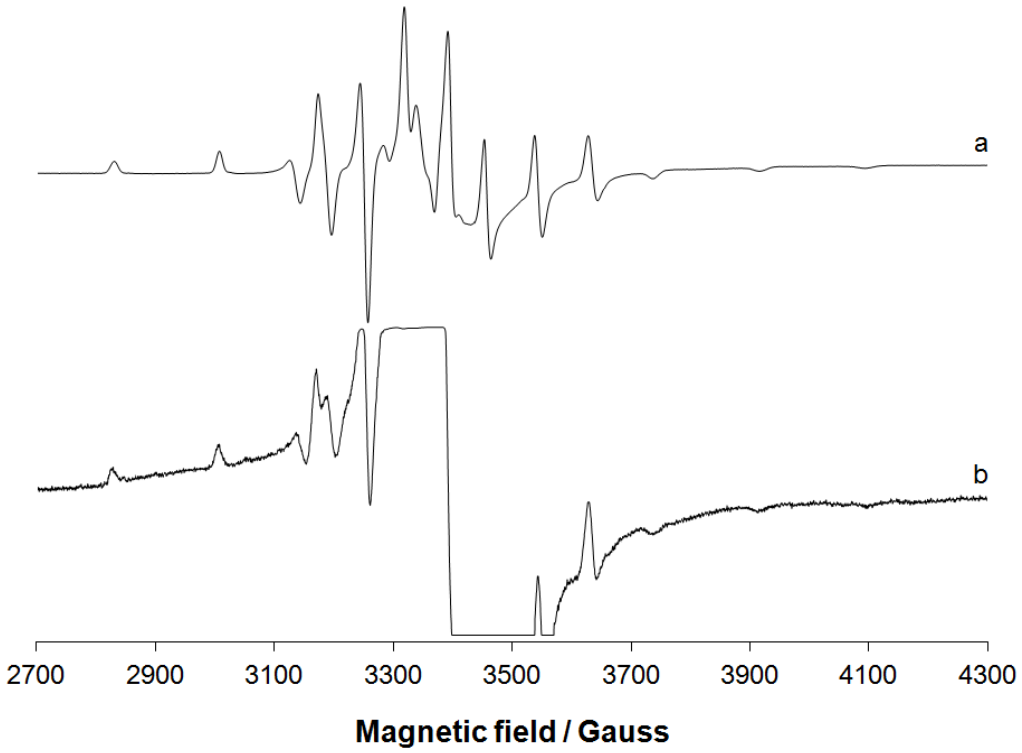

Figure 7. First derivative X-band anisotropic EPR spectra recorded in the systems where $[V^{IV}(L^3)_2]$ (**3**) is dissolved in: (a) phosphate buffer (pH 7.4) and (b) in water (pH 5.0).

Study of protein interaction through docking analysis

The docking analysis for the covalent binding was carried out for the $V^{V}O_2$ species $[V^{V}O_2(L^1)]^-$ (**1'**) and $V^{IV}O$ species $[V^{IV}O(L^2)(H_2O)]$ (**2'**) and $[V^{IV}O(L^3)(H_2O)]$ (**3'**), postulating that proteins (ubiquitin and lysozyme) replace the monodentate water ligand through an amino acid side-chain donor forming a coordination bond, according to the reaction (4):

$$[V^{IV}O(L^{2\text{-}3})(H_2O)] + \text{Protein} \rightarrow V^{IV}O(L^{2\text{-}3})(\text{Protein}) + H_2O \quad (4)$$

The possibility that $[V^{V}O_2(L^1)]^-$ could bind to proteins through a covalent bond to give a hexa-coordinated adduct $V^{V}O_2(L^1)(\text{Protein})$, has been taken into account computationally evaluating – at DFT level of theory and including the solvent effects with SMD model [69] – the relative stability of $[V^{V}O_2(L^1)]^-$ and of the species $[V^{V}O_2(L^1)(\text{MeIm})]^-$ and $[V^{V}O_2(L^1)(\text{AcO})]^{2-}$, where MeIm and AcO^- represent 1-methylimidazole and acetate ion, as models for the binding of His-N or Asp/Glu-COO (eq. 5).

$$[V^{V}O_2(L^1)]^- + \text{MeIm/AcO}^- \rightleftarrows [V^{V}O_2(L^1)(\text{MeIm/AcO}^-)]^{(-/2-)} \quad (5)$$

Only for the complex formed by MeIm it was possible to find an energy minimum, while AcO^- is not stable at the axial site, as it was determined for water (see "ESI Mass Spectrometry" section). However, ΔG_{aq} for the formation of $[V^{V}O_2(L^1)(\text{MeIm})]^-$ is 15.7 kcal/mol, indicating that, for MeIm as well, the possible formation of the 6-coordinated species in solution must be discarded. These data allow to exclude the direct coordination, through a covalent bond, of a protein donor to $[V^{V}O_2(L^1)]^-$ to give a hexa-coordinated species; so, only the non-covalent bond of $[V^{V}O_2(L^1)]^-$ with a closed coordination sphere was considered during the docking calculations (see below).

With Ub, the results indicated that there are several solvent exposed side-chain donors potentially able to bind vanadium. The scoring *F* and population, suggested by docking methods for the potential adducts, are listed in **Table 3**.

Table 3. Proposed binding sites for the covalent binding to ubiquitin of $[V^{IV}O(L^2)(H_2O)]$ (**2'**) and $[V^{IV}O(L^3)(H_2O)]$ (**3'**) suggested by docking methods.[a]

Complex	Residue	V–D/Å	Second interactions	F_{max} [b]	F_{mean} [c]	Pop./% [d]
$[V^{IV}O(L^2)(H_2O)]$	**Glu18**[e]	2.450	Lys29···VO, Lys29···OH	59.1	54.6	18.2
	Asp21[e]	2.110	Lys29···VO, Lys29···OH	56.4	55.3	1.7
	Glu16[e]	2.290	Lys29···VO, Lys29···OH	50.8	51.1	34.8
	Glu51[f]	2.440	Arg72···OH	48.3	41.3	21.0
	His68	2.280	Thr12···OH	47.1	42.4	14.4
	Asp52[f]	2.150	Arg72···OH	40.3	39.7	9.9
$[V^{IV}O(L^3)(H_2O)]$	**Asp21**[e]	2.424	Lys29···VO, Glu16···H_2N	53.8	46.0	20.3
	His68	1.968	–	52.3	41.2	11.5
	Glu51[f]	2.198	Gln49···N–N	46.7	41.3	32.4
	Glu16[e]	2.508	Lys29···VO	45.0	44.1	16.9
	Glu18[e]	2.259	Lys29···VO, Glu16···NH_2	44.1	46.5	16.2
	Asp52[f]	1.941	Glu51···NH_2	37.8	35.1	2.7

[a] The preferential binding sites are highlighted in boldface. [b] GoldScore *Fitness* value obtained for the most stable pose of each cluster (F_{max}). [c] Average value of GoldScore *Fitness* for each cluster (F_{mean}). [d] Percentage computed considering the total of the solutions reported (numbers of solutions per cluster). [e] The binding of Glu16, Glu18 and Asp21 is incompatible with each other. [f] The binding of Glu51 and Asp52 is incompatible with each other.

The best docking proposals were found for the coordination of Asp/Glu-O and His-N of: i) Glu18 or Asp21 and Glu51 or His68 for **2'**; and ii) Glu16 or Asp21 and His68 for **3'**. The best solutions for each complex are shown in **Figure 8**. It is relevant to note that the preferred binding sites are different for the two moieties: Glu18 for $V^{IV}O(L^2)$ and Asp21 for $V^{IV}O(L^3)$, respectively (**Figure 8**). Moreover, because of the three-dimensional disposition of amino acids and large size of the complexes, the simultaneous binding of Glu16, Glu18 or Asp21 residues on one hand, and Glu51 and Asp52 on the other are incompatible. These sites are the same individuated recently for the interaction of $V^{IV}OL_2$ potential drugs with Ub.[25,80] Each adduct appears to be stabilized by at least one hydrogen bond with the surrounding amino acids; in particular, the $–NH_3^+$ of Lys, –NH of Arg, –OH of Thr and $–COO^–$ of Glu are engaged in contacts with the V=O group or –OH, –N–N and $-NH_2$ functionalities of the

ligands.

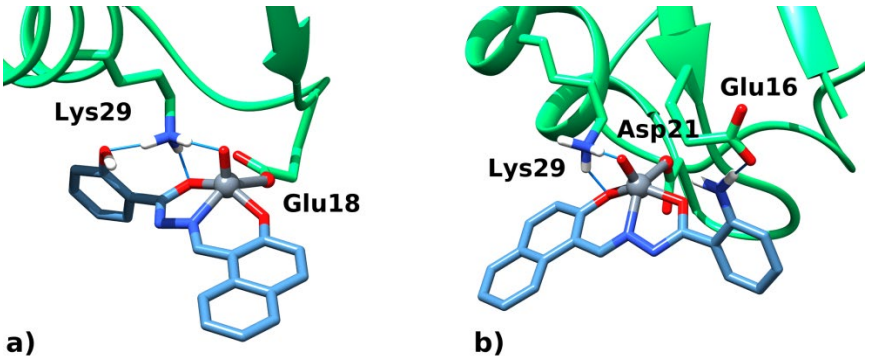

Figure 8. Best docking solutions for the covalent binding of $V^{IV}O$-moieties derived from complexes **2-3** to ubiquitin: (a) $V^{IV}O(L^{2})$ (**2'**) and (b) $V^{IV}O(L^{3})$ (**3'**). Glu18 and Asp21 replaces the water ligand of $[V^{IV}O(L^{2\text{-}3})(H_2O)]$ (**2'** and **3'**). V atom is shown with the grey ball, while hydrogen bonds are depicted as blue thin lines.

Concerning the non-covalent interaction with ubiquitin of penta-coordinated $[V^{V}O_2(L^{1})]^{-}$ (**1'**) and hexa-coordinated non-oxido V^{IV} complexes $[V^{IV}(L^{2\text{-}3})_2]$ (**2** and **3**), only for **1'** and **2** a stable interaction is expected. For these complexes, in fact, F_{max} of the solutions at the interface between the α1, β3, β4 and the C-terminus subunits reaches values higher than 15 GoldScore units. In a recent paper, some of us demonstrated that – using a modified version of GoldScore – only for values larger than 16-17 units the complexes are blocked with a strong interaction (for $V^{IV}O$-flavonoid species it is strong enough to cause the transition from an isotropic to an anisotropic EPR signal at room temperature).[18] The structures, depicted in **Figure 9**, are stabilized by several hydrogen bonds between i) the aza functionality of L^{2} and the charged Arg72 side chain, ii) the oxido ligands of **1'** and the charged Arg72, Arg42, Lys26 or Gln49 side chains and iii) the non-coordinating phenolic group of $L^{1\text{-}2}$ and the carboxylate group of Glu 51 or quaternary nitrogen of Lys27 (**Figure 9**).

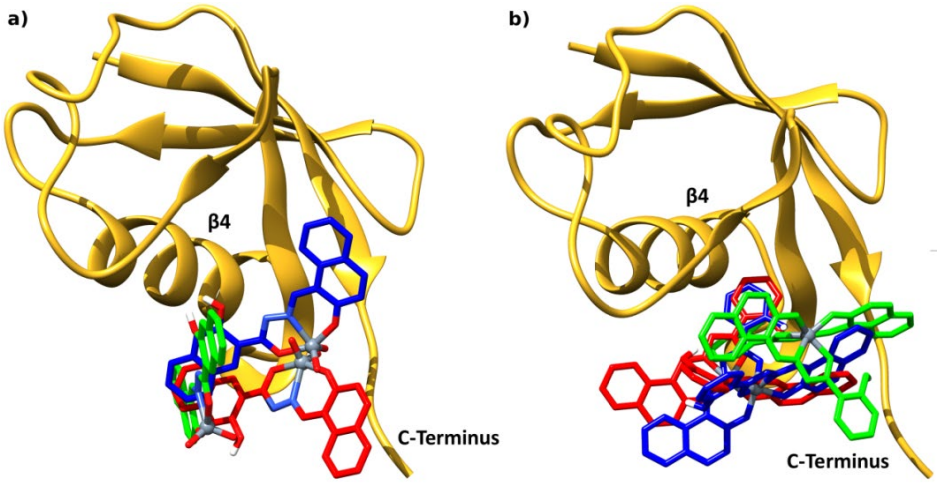

Figure 9. Best representative solutions of the three first clusters (in red, green and blue) for the non-covalent interaction with ubiquitin of: (a) $[V^{V}O_2(L^1)]^-$ (**1'**) and (b) $[V^{IV}(L^2)_2]$ (**2**).

Similarly to ubiquitin, lysozyme presents several exposed amino acids that can potentially act as coordinating residues to bind covalently to the oxidovanadium(IV) species **2'** and **3'**. The docking solutions, summarized in **Table 4**, show appreciable F_{max} values and population.

Table 4. Proposed binding sites for the covalent binding to lysozyme of $[V^{IV}O(L^2)(H_2O)]$ (**2'**) and $[V^{IV}O(L^3)(H_2O)]$ (**3'**) suggested by docking methods.[a]

Complex	Residue	V–D/Å	Second interactions	F_{max} [b]	F_{mean} [c]	Pop./% [d]
$[V^{IV}O(L^2)(H_2O)]$	**His15**	2.206	Thr89···VO	63.1	53.2	40.0
	Glu35	1.888	Asp52···OH	57.5	53.5	60.0
$[V^{IV}O(L^3)(H_2O)]$	**His15**	2.273	Arg14···O	64.9	56.3	41.5
	Asp52[e]	1.808	Val109···N–N	50.4	50.3	1.2
	Glu35[e]	1.931	Asp52···NH_2	58.7	54.5	57.3

[a] The preferential binding sites are highlighted in boldface. [b] GoldScore *Fitness* value obtained for the most stable pose of each cluster (F_{max}). [c] Average value of GoldScore *Fitness* for each cluster (F_{mean}). [d] Percentage computed considering the total of the solutions reported (numbers of solutions per cluster). [e] The binding of Glu35 and Asp52 is incompatible with each other.

On the basis of the docking solutions, the preferential binding sites for the two moieties $V^{IV}O(L^2)$ and $V^{IV}O(L^3)$ should involve the coordination to the V center of the imidazole-N of His15 and of carboxylate-O of Glu35 or Asp52. Similarly to ubiquitin, these adducts are stabilized by at least one hydrogen bond. The most important secondary interactions are between the functionalities NH_2 of Arg or carboxylate of Glu with the V=O or OH groups of the ligands. The best docking solution for each complex is reported in **Figure 10**.

Differently from ubiquitin, the most stable adducts of $V^{IV}O(L^2)$ and $V^{IV}O(L^3)$ with lysozyme are formed upon the coordination of only one residue (His15) and with the binding of a nitrogen donor instead of a carboxylate oxygen. Another interesting feature is that lysozyme would bind these $V^{IV}O$ moieties with a mono-chelated (eq-eq-eq) ligand through His15, while it binds the more crowded bis-chelated $V^{IV}O$ fragments having an (eq-eq); (eq-ax) arrangement of the two ligands (for example, picolinate and maltolate) with accessible carboxylate-containing side chains (Asp52, Glu35 or Glu7).[21,105] The reason lies in the fact that His15 is not completely exposed on the protein surface and the steric hindrance of the ligand(s) hinders its binding to vanadium; in contrast, the fourth equatorial position of $V^{IV}O(L^2)$ and $V^{IV}O(L^3)$ is less crowded and the approach of His15 becomes possible.

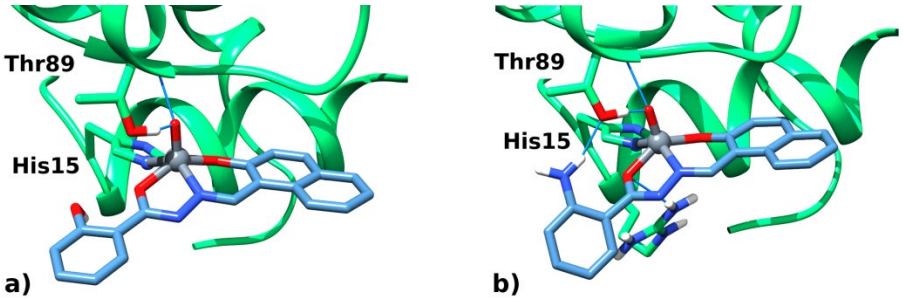

Figure 10. Best docking solutions for the covalent binding of $V^{IV}O$ moieties derived from complexes **2**-**3** with lysozyme: (a) $V^{IV}O(L^2)$ (**2'**) and (b) $V^{IV}O(L^3)$ (**3'**). His15 replaces the water ligand of $[V^{IV}O(L^{2\text{-}3})(H_2O)]$ (**2'** and **3'**). V atom is shown with the grey ball, while hydrogen bonds are depicted as blue thin lines.

As in the systems with ubiquitin, the analysis of the non-covalent surface interaction of the oxido V^{V} **1'** and non-oxido V^{IV} complexes **2** and **3** suggested that only **1'** and **2** form stable adducts. In fact, F_{max} values higher than 15 GoldScore units were obtained. The best docking solutions, depicted in **Figure 11**, are stabilized by hydrogen bonds between the NH group of Trp62 and Trp63, NH_2 of Arg112, CO of Asn109 and COO^- of Asp52 with the phenolic function of the $L^1(2–)$ and $L^2(2–)$ ligands.

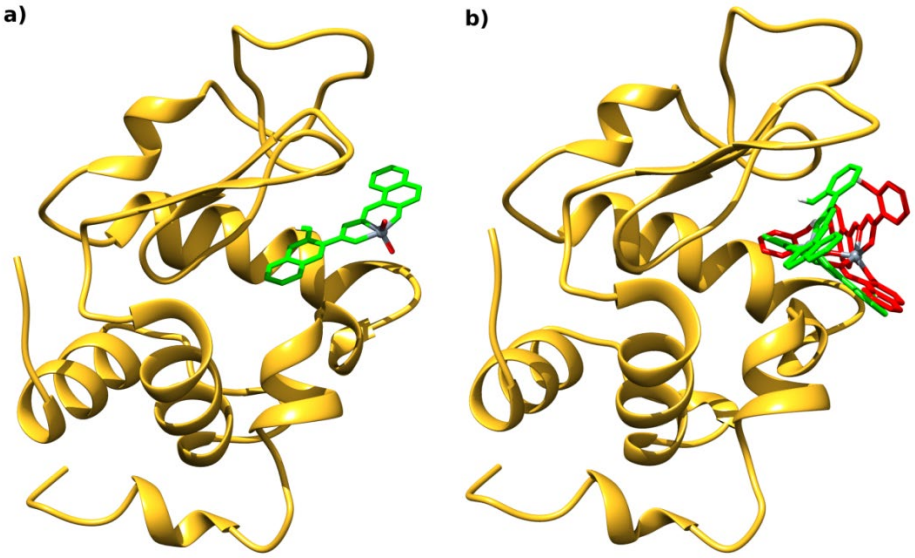

Figure 11. Best representative solutions of the two first clusters (in green and red, respectively) for the non-covalent interaction with lysozyme of: (a) $[V^{V}O_2(L^1)]^-$ (**1'**) and (b) $[V^{IV}(L^2)_2]$ (**2**).

***In vitro* cytotoxicity studies**

The cytotoxic activity of ligand precursors ($H_2L^{1–3}$) and complexes **1-3** was evaluated against the ovarian A2780 and prostate PC3 cancer cells. Concerning pharmacological applications, a relevant characteristic for a prospective anticancer drug is its high degree of specificity for cancer cells, sparing normal cells.[106] In this work, V79 fibroblasts were chosen as a normal

cell line to evaluate the selectivity of the complexes against cancer cells (**Table 5**). As it can be observed from **Table 5** and **Figure 12**, which depicts the dose response curves obtained, the compounds displayed different cytotoxicity against the ovarian cancer cells upon 48 h of exposure in the order **1** > **2** > **3**. Moreover, their cytotoxic activity was shown to be cell type dependent, *i.e.*, they were more active in the ovarian cancer cells than the prostate cells. This result was predictable taking into consideration the highly aggressive behavior of this prostate cell line.[107] For H_2L^1, the coordination to vanadium did not improve its activity; in fact, H_2L^1 is more active than its corresponding complex. On the other hand compound **1** is much more selective for A2780 cells than H_2L^1, IC_{50}: 1.1±0.6 μM and selectivity index (SI) = 19, thus exhibiting important anti-proliferative activity associated with good SI when considering normal fibroblasts. From this strict point of view, compound **1** is the most promising one for A2780 cells. However, beside **1** being converted to **1'** once dissolved in incubation media, its cytotoxicity is probably partly due to its ligand moiety, which has a much lower IC_{50} and SI against A2780 cells. For compounds **2** and **3**, the trend differs from **1**, since both complexes were more active than their corresponding ligand precursors. H_2L^3 was the least active compound.

Recently the anti-proliferative activity of some non-oxidovanadium-catecholate complexes was studied. Besides emphasizing the probable relation between their thermodynamic stabilities and uptake by cells of the intact complex, the relevance of understanding their hydrolysis in solution, and the determination of which is/are the active species for the cytotoxicity was highlighted.[46] In the case of complexes **2**−**3**, in the above sections we showed that there is significant transformation of the non-oxidovanadium complexes **2**−**3** into their corresponding oxidovanadium(IV) species (**2'**−**3'**) in solution (eq. 3); V^VO-species were also detected in ESI-MS. Therefore, we may predict that in incubation media all these species may be present, and this mixture could be responsible for the cytotoxic activity in the

experiments with **2** and **3**.[11] Actually, the situation is more complex as the incubation media contains several potential ligands for vanadium.

Complexes **1** and **2** were less toxic to normal cells than **3**. Considering the data in **Table 5**, although compound **1** is more selective, the corresponding free ligand is quite toxic, thus globally **2** proved to be the most promising complex of the series and deserves to be further explored as anticancer agent, in particular for the ovarian cancer.

Nevertheless, the results of H_2L^2 and complex **2** with V79 fibroblasts are somewhat intriguing. The IC_{50} for the ligand precursor is much lower than for complex **2**; yet, according to eq. 3, for each $[V^{IV}O(L^2)(H_2O)]$ formed, one free ligand is produced that should exert its toxic effect. The maintenance of most of $[V^{IV}(L^2)_2]$, due to its high stability, may probably explain this. When considering non-oxido vanadium complexes, their biological effects are normally attributed to their derivatives $[V^{IV}O(L)(H_2O)]$ (or $[V^{V}O_n(L)]$ with n = 1-2), formed from hydrolysis of the corresponding $[V^{IV}(L)_2]$ precursors.[15] Complex **2** may probably be an exception to this typical behavior. Other examples are amavadine[108] and previously reported V^{IV}-aroylhydrazonato complexes.[44]

Table 5. IC_{50} values (μM) calculated for the ligand precursors and corresponding vanadium complexes against the ovarian and prostate cancer cells, and the normal fibroblasts, upon 48 h of exposure. Results are the mean±SD of two independent experiments done with six replicates.

Compounds	A2780	PC3	V79 (normal cells)
H_2L^1	0.2±0.1	8.7±0.4	2.4±1.1
1	1.1±0.6	17±1.0	21±3.1
H_2L^2	9.7±4.4	28±4.2	3.2±1.1
2	4.5±1.8	15±1.7	14±2.5
H_2L^3	>100	>100	73±18
3	20±3.0	29±5.0	12±2.3

Prevalent chemotherapeutic drug such as cisplatin has shown comparable cytotoxic potential under identical conditions against A2780 and PC3 cancer cell lines with IC_{50} values of 22.4[109] and 51.0 μM,[83] respectively. When the present compounds may be also compared with previously reported $V^{V}O_2$-complexes of NNO donor Schiff base ligands, tested against A2780 and PC3 cancer cell lines (IC_{50} values in the range 7−22 μM),[83] or with with 8-hydroxyquinoline (8HQ) derived vanadium(IV,V) complexes, such as [$V^{IV}O$(pic)(8HQ)] (pic = picolinato), [$V^{IV}O$(sal-Gly)(8HQ)] (sal-Gly = N-salicylideneglycinato), [$V^{V}O$(L-pheolnaph-im)(8HQ)], [$V^{V}O$(L-pheolnaph-im)(5-Cl-8HQ)] (nath-Phe = N-naththalidene-L-phenylalaninato), and [$V^{V}O$(MeO)$(8HQ)_2$]) (IC_{50} values in the range 5.4−14.0 μM)[109] as well as with mixed ligand vanadium(IV) complexes of salicylaldimines [VO(sal-Gly)(bipy)], [VO(sal-Gly)(phen)] [VO(sal-L-Phe)(H_2O)], [VO(sal-L-Phe)(bipy)] and [VO(sal-L-Phe)(phen)] (sal-Phe = N-salicylidene-L-phenylalaninato, bipy = 2,2'-bipyridine, phen = 1,10-phenanthroline) (IC_{50} values between 4.7 and 20.8 μM)[110] have been tested. The complexes herein studied showed similar, or in some cases improved *in vitro* cytotoxicity, when compared with our previously reported vanadium systems against different cancer cell lines such as HeLa (cervical), HT-29 (colorectal) and A549 (lung).[34,37–39,44]

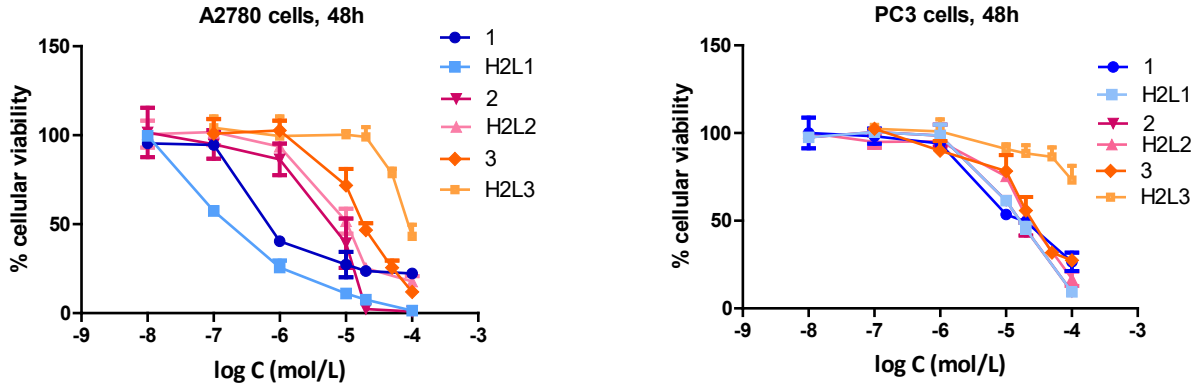

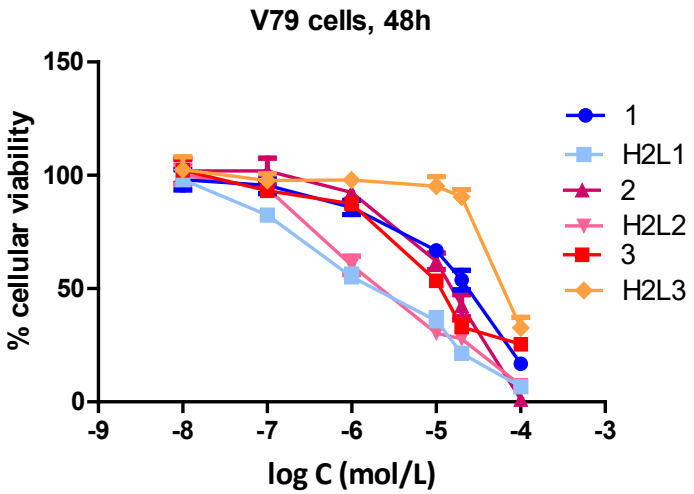

Figure 12. Dose response curves obtained by the GraphPad Prism software (*vs* 5.0) for the effect of ligand precursors (H_2L^{1-3}) and respective complexes (**1-3**).

CONCLUSIONS

Three aroylhydrazones H_2L^{1-3} and corresponding vanadium complexes, one oxido $[V^{V}O(L^{1})(OEt)]$ (**1**) and two non-oxido compounds, $[V^{IV}(L^{2-3})]$ (**2** and **3**) were prepared and characterized by several physicochemical techniques, including single-crystal X-ray diffraction. DFT methodologies were used to model both their UV-Vis and EPR spectra; besides the good agreement between the experimental and DFT-calculated data, it was shown that the relatively strong bands observed for the non-oxido V^{IV}-complexes **2** and **3** in the visible range mainly correspond to LMCT transitions.

All complexes and free ligands were evaluated for their anti-proliferative activity against ovarian (A2780) and prostate (PC3) human cancer cells, as well as in normal fibroblasts (V79). While H_2L^1 is significantly more active than its corresponding complexes **1** (and/or **1'**), the non-oxido complexes **2** and **3**, and particularly **3** are more active than their ligand precursors H_2L^2 and H_2L^3. In aqueous solution the non-oxido V^{IV}-complexes **2** and **3** are

partly converted to the corresponding $V^{IV}O$-complexes $[V^{IV}O(L^{2-3})(H_2O)]$ (indicated with **2'** and **3'**), and probably to a V^{V}-complex; therefore, the cytotoxicity measured for complexes **2** and **3** is due to the presence of several species: the non-oxido complexes, their corresponding $V^{IV,V}$-complexes and the free ligands. Since any of these species may bind to components of cell media, namely to BSA, thus the cytotoxic action may be due to many distinct factors.

Once uptaken by cells, the compounds may bind to enzymes/proteins somewhat affecting their role in biological processes. By the use of docking procedures with lysozime and ubiquitin, we showed that non-oxidovanadium complex **2**, as well as the oxidovanadium(IV,V) derivatives (**1'**, **2'** and **3'**) may bind to proteins both with covalent (coordination) bonds or non-covalent interactions on the protein surface. His-N and Asp/Glu-COO^- are the preferential donors, mainly when the binding is stabilized by secondary interactions.

Thus, interaction with proteins critical for the survival of the cells may be relevant to explain the cytotoxic action of the compounds, these being factors that should be evaluated when attempting to access mechanisms of biological action of vanadium compounds.

ASSOCIATED CONTENT

Supporting Information

The Supporting Information and crystallographic data in CIF format is available free of charge at DOI: XXXXX.

Packing structure of molecules **1** (**Figure S1**), Crystal data and structure refinement details for compounds **1**-**3** (**Table S1**) and their selected geometric parameters (**Table S2A** and **S2B**). ESI-MS spectrum of **1** (**Figures S2**-**S3** and **Tables S3**-**S4**) and **2** (**Figures S4**-**S7** and **Tables S5**-**S6**), UV-Vis spectra of **1**–**3** (**Figures S8-S9**), NMR spectra of **1** (**Figures S10-S12**) and cathodic and anodic scans for H_2L^1 (**Figures S13**).

AUTHOR INFORMATION

Corresponding Authors

*E-mail: rupamdinda@nitrkl.ac.in (Rupam Dinda)

*E-mail: garribba@uniss.it (Eugenio Garribba)

*Email: joao.pessoa@ist.utl.pt (João Costa Pessoa)

ORCID

Rupam Dinda: 0000-0001-9452-7791

Eugenio Garribba: 0000-0002-7229-5966

João Costa Pessoa: 0000-0002-3978-9964

Giuseppe Sciortino: 0000-0001-9657-1788

Fernanda Carvalho: 0000-0002-6825-1696

Fernanda Marques: 0000-0001-8440-5299

Werner Kaminsky: 0000-0002-9100-4909

Krzysztof Brzezinski: 0000-0001-9339-7745

Author Contributions

The manuscript was written through contributions of all authors. All authors have given approval to the final version of the manuscript.

Notes

The authors declare no competing financial interest.

ACKNOWLEDGMENTS

R. D. thanks CSIR, Govt. of India [Grant No. 01(2963)/18/EMR-II] for funding this research. E.G. and G.S. are grateful to Regione Autonoma della Sardegna (grant RASSR79857) and Università di Sassari (fondo di Ateneo per la ricerca 2019) for the financial support. This work was also supported by *Fundação para a Ciência e Tecnologia* (FCT) (projects

UIDB/00100/2020, RECI/QEQ-QIN/0189/2012, RECI/QEQ-MED/0330/2012, UID/Multi/04349/2019), *Programa Operacional Regional de Lisboa* (LISBOA-01-0145-FEDER-007317). The Portuguese NMR and Mass Spectrometry IST-UL Centres are acknowledged for the access to the equipment. The authors also thank Dr. Isabel Correia for recording ^{51}V NMR, EPR and circular dichroism data. W. K. is grateful to the Department of Chemistry, Univ. of Washington for access to the X-ray facility, funded by NSF Grant 0840520.

REFERENCES

(1) Kioseoglou, E.; Petanidis, S.; Gabriel, C.; Salifoglou, A. The chemistry and biology of vanadium compounds in cancer therapeutics. *Coord. Chem. Rev.* **2015**, *301-302*, 87–105.

(2) Pessoa, J. C.; Etcheverry, S.; Gambino, D. Vanadium compounds in medicine. *Coord. Chem. Rev.* **2015**, *301*, 24–48.

(3) Gambino, D. Potentiality of vanadium compounds as anti-parasitic agents. *Coord. Chem. Rev.* **2011**, *255*, 2193–2203.

(4) Crans, D. C.; Yang, L.; Haase, A.; Yang, X. Health benefits of vanadium and its potential as an anticancer agent. *Met. Ions Life Sci* **2018**, *18*, 251–279.

(5) Mjos, K. D.; Orvig, C. Metallodrugs in medicinal inorganic chemistry. *Chem. Rev.* **2014**, *114*, 4540–4563.

(6) Pessoa, J. C.; Garribba, E.; Santos, M. F. A.; Santos-Silva, T. Vanadium and proteins: Uptake, transport, structure, activity and function. *Coord. Chem. Rev.* **2015**, *301-302*, 49–86.

(7) Jakusch, T.; Hollender, D.; Enyedy, É. A.; González, C. S.; Montes-Bayón, M.; Sanz-Medel, A.; Pessoa, J. C.; Tomaz, I.; Kiss, T. Biospeciation of various antidiabetic $V^{IV}O$ compounds in serum. *Dalton Trans.* **2009**, 2428–2437.

(8) Sanna, D.; Micera, G.; Garribba, E. Interaction of insulin-enhancing vanadium compounds with human serum holo-transferrin. *Inorg. Chem.* **2013**, *52*, 11975–11985.

(9) Pessoa, J. C.; Gonçalves, G.; Roy, S.; Correia, I.; Mehtab, S.; Santos, M. F. A.; Santos-Silva, T. New insights on vanadium binding to human serum transferrin. *Inorganica Chim. Acta* **2014**, *420*, 60–68.

(10) Levina, A.; McLeod, A. I.; Gasparini, S. J.; Nguyen, A.; Silva, W. M. de; Aitken, J. B.; Harris, H. H.; Glover, C.; Johannessen, B.; Lay, P. A. Reactivity and speciation of anti-diabetic vanadium complexes in whole blood and its components: the important role of red blood cells. *Inorg. Chem.* **2015**, *54*, 7753–7766.

(11) Sanna, D.; Palomba, J.; Lubinu, G.; Buglyó, P.; Nagy, S.; Perdih, F.; Garribba, E. Role of Ligands in the Uptake and Reduction of V(V) Complexes in Red Blood Cells. *J. Med. Chem.* **2019**, *62*, 654–664.

(12) Sanna, D.; Ugone, V.; Serra, M.; Garribba, E. Speciation of potential anti-diabetic vanadium complexes in real serum samples. *J. Inorg. Biochem.* **2017**, *173*, 52–65.

(13) Crans, D. C.; Tarlton, M. L.; McLauchlan, C. C. Trigonal Bipyramidal or Square Pyramidal Coordination Geometry? Investigating the Most Potent Geometry for Vanadium Phosphatase Inhibitors. *Eur. J. Inorg. Chem.* **2014**, *2014*, 4450–4468.

(14) McLauchlan, C. C.; Peters, B. J.; Willsky, G. R.; Crans, D. C. Vanadium–phosphatase complexes: phosphatase inhibitors favor the trigonal bipyramidal transition state geometries. *Coord. Chem. Rev.* **2015**, *301*, 163–199.

(15) Yoshikawa, Y.; Sakurai, H.; Crans, D. C.; Micera, G.; Garribba, E. Structural and redox requirements for the action of anti-diabetic vanadium compounds. *Dalton Trans.* **2014**, *43*, 6965–6972.

(16) Pagadala, N. S.; Syed, K.; Tuszynski, J. Software for molecular docking: a review. *Biophys. Rev.* **2017**, *9*, 91–102.

(17) Riccardi, L.; Genna, V.; Vivo, M. de. Metal–ligand interactions in drug design. *Nat. Rev. Chem.* **2018**, *2*, 100–112.

(18) Sciortino, G.; Sanna, D.; Ugone, V.; Lledós, A.; Maréchal, J.-D.; Garribba, E. Decoding Surface Interaction of $V^{IV}O$ Metallodrug Candidates with Lysozyme. *Inorg. Chem.* **2018**, *57*, 4456–4469.

(19) Sciortino, G.; Garribba, E.; Rodríguez-Guerra Pedregal, J.; Maréchal, J.-D. Simple Coordination Geometry Descriptors Allow to Accurately Predict Metal-Binding Sites in Proteins. *ACS Omega* **2019**, *4*, 3726–3731.

(20) Sciortino, G.; Rodríguez-Guerra Pedregal, J.; Lledós, A.; Garribba, E.; Maréchal, J.-D. Prediction of the interaction of metallic moieties with proteins: An update for protein-ligand docking techniques. *J. Comput. Chem.* **2018**, *39*, 42–51.

(21) Sciortino, G.; Sanna, D.; Ugone, V.; Micera, G.; Lledós, A.; Maréchal, J.-D.; Garribba, E. Elucidation of Binding Site and Chiral Specificity of Oxidovanadium Drugs with Lysozyme through Theoretical Calculations. *Inorg. Chem.* **2017**, *56*, 12938–12951.

(22) Sciortino, G.; Garribba, E.; Maréchal, J.-D. Validation and Applications of Protein–Ligand Docking Approaches Improved for Metalloligands with Multiple Vacant Sites. *Inorg. Chem.* **2019**, *58*, 294–306.

(23) Balsells, J.; Mejorado, L.; Phillips, M.; Ortega, F.; Aguirre, G.; Somanathan, R. P.; Walsh, J. Synthesis of chiral sulfonamide/Schiff base ligands. *Tetrahedron Asymm.* **1998**, *9*, 4135–4142.

(24) Sima, J. Mechanism of Photoredox Reactions of Iron(III) Complexes Containing Salen-type Ligands **2001**, *74*, 593-600.

(25) Sciortino, G.; Sanna, D.; Ugone, V.; Maréchal, J.-D.; Alemany-Chavarria, M.; Garribba, E. Effect of secondary interactions, steric hindrance and electric charge on the interaction of $V^{IV}O$ species with proteins. *New J. Chem.* **2019**, *43*, 17647–17660.

(26) Campbell, M. J. M. Transition metal complexes of thiosemicarbazide and thiosemicarbazones. *Coord. Chem. Rev.* **1975**, *15*, 279–319.

(27) Terra, L. H. S. Á.; da Cunha Areias, M. C.; Gaubeur, I.; Encarnación, M.; Suárez-iha, V. Solvent Extraction-Spectrophotometric Determination of Nickel(II) in Natural Waters Using DI-2-Pyridyl Ketone Benzoylhydrazone. *Spectrosc. Lett.* **1999**, *32*, 257–271.

(28) Cui, Z.; Yang, X.; Shi, Y.; Uzawa, H.; Cui, J.; Dohi, H.; Nishida, Y. Molecular design, synthesis and bioactivity of glycosyl hydrazine and hydrazone derivatives: Notable effects of the sugar moiety. *Bioorg. Med. Chem. Lett.* **2011**, *21*, 7193–7196.

(29) Maurya, M. R.; Agarwal, S.; Abid, M.; Azam, A.; Bader, C.; Ebel, M.; Rehder, D. Synthesis, characterisation, reactivity and in vitro antiamoebic activity of hydrazone based oxovanadium(IV), oxovanadium(V) and μ-bis(oxo)bisoxovanadium(V) complexes. *Dalton Trans.* **2006**, 937–947.

(30) Savini, L.; Chiasserini, L.; Travagli, V.; Pellerano, C.; Novellino, E. New α-(N)-heterocyclichydrazones: evaluation of anticancer, anti-HIV and antimicrobial activity. *Eur. J. Med.* **2004**, *39*, 113–122.

(31) Biswas, N.; Bera, S.; Sepay, N.; Pal, A.; Halder, T.; Ray, S.; Acharyya, S.; Biswas, A. K.; Drew, M. G. B.; Ghosh, T. Simultaneous formation of non-oxidovanadium (IV) and oxidovanadium (V) complexes incorporating phenol-based hydrazone ligands in aerobic conditions. *New J. Chem.* **2020**, *44*, 3700–3716.

(32) Dinda, R.; Majhi, P. K.; Sengupta, P.; Pasayat, S.; Ghosh, S.; Falvello, L. R.; Mak, T. C. W. Alkali metal (Na^+ and K^+)-mediated supramolecular assembly of oxovanadium(V) complexes: Synthesis and structural characterization. *Polyhedron* **2010**, *29*, 248–253.

(33) Dash, S. P.; Pasayat, S.; Saswati; Dash, H. R.; Das, S.; Butcher, R. J.; Dinda, R. Oxovanadium(V) complexes incorporating tridentate aroylhydrazoneoximes: Synthesis, characterizations and antibacterial activity. *Polyhedron* **2012**, *31*, 524–529.

(34) Dash, S. P.; Panda, A. K.; Pasayat, S.; Dinda, R.; Biswas, A.; Tiekink, E. R. T.; Patil, Y. P.; Nethaji, M.; Kaminsky, W.; Mukhopadhyay, S.; Bhutia, S. K. Syntheses and structural investigation of some alkali metal ion-mediated LV^VO^{2-} (L^{2-} = tridentate ONO ligands) species: DNA binding, photo-induced DNA cleavage and cytotoxic activities. *Dalton Trans.* **2014**, *43*, 10139–10156.

(35) Dash, S. P.; Panda, A. K.; Pasayat, S.; Dinda, R.; Biswas, A.; Tiekink, E. R. T.; Mukhopadhyay, S.; Bhutia, S. K.; Kaminsky, W.; Sinn, E. Oxidovanadium(V) complexes of aroylhydrazones incorporating heterocycles: synthesis, characterization and study of DNA binding, photo-induced DNA cleavage and cytotoxic activities. *RSC Adv.* **2015**, *5*, 51852–51867.

(36) Dash, S. P.; Panda, A. K.; Dhaka, S.; Pasayat, S.; Biswas, A.; Maurya, M. R.; Majhi, P. K.; Crochet, A.; Dinda, R. A study of DNA/BSA interaction and catalytic potential of

oxidovanadium(v) complexes with ONO donor ligands. *Dalton Trans.* **2016**, *45*, 18292–18307.

(37) Mohanty, M.; Maurya, S. K.; Banerjee, A.; Patra, S. A.; Maurya, M. R.; Crochet, A.; Brzezinski, K.; Dinda, R. In vitro cytotoxicity and catalytic evaluation of dioxidovanadium(v) complexes in an azohydrazone ligand environment. *New J. Chem.* **2019**, *43*, 17680–17695.

(38) Roy, S.; Böhme, M.; Dash, S. P.; Mohanty, M.; Buchholz, A.; Plass, W.; Majumder, S.; Kulanthaivel, S.; Banerjee, I.; Reuter, H.; Kaminsky, W.; Dinda, R. Anionic Dinuclear Oxidovanadium(IV) Complexes with Azo Functionalized Tridentate Ligands and μ-Ethoxido Bridge Leading to an Unsymmetric Twisted Arrangement: Synthesis, X-ray Structure, Magnetic Properties, and Cytotoxicity. *Inorg. Chem.* **2018**, *57*, 5767–5781.

(39) Lima, S.; Banerjee, A.; Mohanty, M.; Sahu, G.; Kausar, C.; Patra, S. K.; Garribba, E.; Kaminsky, W.; Dinda, R. Synthesis, structure and biological evaluation of mixed ligand oxidovanadium(V) complexes incorporating 2-(arylazo)phenolates. *New J. Chem.* **2019**, 17711–17725.

(40) Banerjee, A.; Dash, S. P.; Mohanty, M.; Sanna, D.; Sciortino, G.; Ugone, V.; Garribba, E.; Reuter, H.; Kaminsky, W.; Dinda, R. Chemistry of mixed-ligand oxidovanadium(IV) complexes of aroylhydrazones incorporating quinoline derivatives: Study of solution behavior, theoretical evaluation and protein/DNA interaction. *J. Inorg. Biochem.* **2019**, 110786.

(41) Dinda, R.; Sengupta, P.; Ghosh, S.; Mak, T. C. W. Valence Delocalization in a Mixed-Oxidation Divanadium (IV, V) Complex Electrogenerated from Its Structurally Characterized Divanadium (V) Analogue with a Tridentate (ONO) Ligand. *Inorg. Chem.* **2002**, *41*, 1684–1688.

(42) Dinda, R.; Sengupta, P.; Sutradhar, M.; Mak, T. C. W.; Ghosh, S. Solution study of a structurally characterized monoalkoxo-bound monooxo-vanadium(V) complex: spontaneous generation of the corresponding oxobridged divanadium(V,V) complex and its electroreduction to a mixed-valence species in solution. *Inorg. Chem.* **2008**, *47*, 5634–5640.

(43) Dash, S. P.; Roy, S.; Mohanty, M.; Carvalho, M. F. N. N.; Kuznetsov, M. L.; Pessoa, J. C.; Kumar, A.; Patil, Y. P.; Crochet, A.; Dinda, R. Versatile Reactivity and Theoretical Evaluation of Mono- and Dinuclear Oxidovanadium(V) Compounds of Aroylazines:

Electrogeneration of Mixed-Valence Divanadium(IV,V) Complexes. *Inorg. Chem.* **2016**, *55*, 8407–8421.

(44) Dash, S. P.; Pasayat, S.; Bhakat, S.; Roy, S.; Dinda, R.; Tiekink, E. R. T.; Mukhopadhyay, S.; Bhutia, S. K.; Hardikar, M. R.; Joshi, B. N.; Patil, Y. P.; Nethaji, M. Highly stable hexacoordinated nonoxidovanadium(IV) complexes of sterically constrained ligands: syntheses, structure, and study of antiproliferative and insulin mimetic activity. *Inorg. Chem.* **2013**, *52*, 14096–14107.

(45) Dash, S. P.; Majumder, S.; Banerjee, A.; Carvalho, M. F. N. N.; Adão, P.; Pessoa, J. C.; Brzezinski, K.; Garribba, E.; Reuter, H.; Dinda, R. Chemistry of Monomeric and Dinuclear Non-Oxido Vanadium(IV) and Oxidovanadium(V) Aroylazine Complexes: Exploring Solution Behavior. *Inorg. Chem.* **2016**, *55*, 1165–1182.

(46) Griffin, E.; Levina, A.; Lay, P. A. Vanadium (V) tris-3, 5-di-tert-butylcatecholato complex: Links between speciation and anti-proliferative activity in human pancreatic cancer cells. *J. Inorg. Biochem.* **2019**, *201*, 110815.

(47) Crans, D. C.; Koehn, J. T.; Petry, S. M.; Glover, C. M.; Wijetunga, A.; Kaur, R.; Levina, A.; Lay, P. A. Hydrophobicity may enhance membrane affinity and anti-cancer effects of Schiff base vanadium (V) catecholate complexes. *Dalton Trans.* **2019**, *48*, 6383–6395.

(48) Levina, A.; Crans, D. C.; Lay, P. A. Speciation of metal drugs, supplements and toxins in media and bodily fluids controls in vitro activities. *Coord. Chem. Rev.* **2017**, *352*, 473–498.

(49) Korbecki, J.; Baranowska-Bosiacka, I.; Gutowska, I.; Chlubek, D. Biochemical and medical importance of vanadium compounds. *Acta Biochim. Polon.* **2012**, *59*, 195–200.

(50) Dankhoff, K.; Ahmad, A.; Weber, B.; Biersack, B.; Schobert, R. Anticancer properties of a new non-oxido vanadium (IV) complex with a catechol-modified 3, 3′-diindolylmethane ligand. *J. Inorg. Biochem.* **2019**, *194*, 1–6.

(51) Bryant, B. E.; Fernelius, W. C.; Busch, D. H.; Stoufer, R. C.; Stratton, W. Vanadium(IV) Oxy(acetylacetonate). *Inorganic Syntheses*; Inorganic Syntheses; John Wiley & Sons, Inc: Hoboken, NJ, USA, 1957; pp 113–116.

(52) Armarego, W. L. F.; Chai, C. L. L. *Purification of Laboratory Chemicals*, Sixth Edition; Elsevier; Butterworth Heinemann: Amsterdam, Boston, Paris, op. 2009.

(53) *WINEPR SimFonia, version 1.25*; Bruker Analytische Messtechnik GmbH, Karlshrue, 1996.

(54) Pasayat, S.; Dash, S. P.; Roy, S.; Dinda, R.; Dhaka, S.; Maurya, M. R.; Kaminsky, W.; Patil, Y. P.; Nethaji, M. Synthesis, structural studies and catalytic activity of dioxidomolybdenum(VI) complexes with aroylhydrazones of naphthol-derivative. *Polyhedron* **2014**, *67*, 1–10.

(55) Bruker (2007) APEX2 (Version 2.1-4), SAINT (version 7.34A), SADABS (version 2007/4), BrukerAXS Inc, Madison, Wisconsin, USA.

(56) Otwinowski, Z.; Minor, W. *In: Methods in Enzymology, Vol. 276, Macromolecular Crystallography, Part A, edited by CW Carter Jr & RM Sweet*; New York: Academic Press, 1997.

(57) Altomare, A.; Burla, M. C.; Camalli, M.; Cascarano, G. L.; Giacovazzo, C.; Guagliardi, A.; Moliterni, A. G. G.; Polidori, G.; Spagna, R. SIR 97: a new tool for crystal structure determination and refinement. *J. Appl. Cryst.* **1999**, *32*, 115–119.

(58) Sheldrick, G. M. SHELXT - integrated space-group and crystal-structure determination. *Acta Crystallogr. Sect. A* **2015**, *71*, 3–8.

(59) Sheldrick, G. M. SHELXL-97: Program for the Refinement of Crystal Structures 1997 University of Gottingen, Germany.

(60) Sheldrick, G. M. Crystal structure refinement with SHELXL. *Acta Crystallogr. Sect. C* **2015**, *71*, 3–8.

(61) Waasmaier, D.; Kirfel, A. New analytical scattering-factor functions for free atoms and ions. *Acta Crystallographica A.* **1995**, *51*, 416–431.

(62) Dolomanov, O. V.; Bourhis, L. J.; Gildea, R. J.; Howard, J. A. K.; Puschmann, H. OLEX2 : a complete structure solution, refinement and analysis program. *J Appl Crystallogr* **2009**, *42*, 339–341.

(63) Spek, A. L. Structure validation in chemical crystallography. *Acta Crystallogr. Sect. D: Biol. Crystallogr.* **2009**, *65*, 148–155.

(64) Frisch, M. J.; Trucks, G. W.; Schlegel, H. B.; Scuseria, G. E.; Robb, M. A.; Cheeseman, J. R.; Scalmani, G.; Barone, V.; Mennucci, B.; Petersson, G. A.; Nakatsuji, H.; Caricato, M.; Li, X.; Hratchian, H. P.; Izmaylov, A. F.; Bloino, J.; Zheng, G.; Sonnenberg, J. L.; Hada, M.; Ehara, M.; Toyota, K.; Fukuda, R.; Hasegawa, J.; Ishida, M.; Nakajima, T.; Honda, Y.; Kitao, O.; Nakai, H.; Vreven, T.; Montgomery, J. A.; Jr., Peralta, J. E.; Ogliaro, F.; Bearpark, M.; Heyd, J. J.; Brothers, E.; Kudin, K. N.; Staroverov, V. N.; Keith, T.; Kobayashi, R.; Normand, J.; Raghavachari, K.; Rendell, A.; Burant, J. C.; Iyengar, S. S.; Tomasi, J.; Cossi, M.; Rega, N.; Millam, J. M.; Klene, M.; Knox, J. E.; Cross, J. B.; Bakken,V.; Adamo, C.; Jaramillo, J.; Gomperts, R.; Stratmann, R. E.; Yazyev, O.; Austin, A. J.; Cammi, R.; Pomelli, C.; Ochterski, J. W.; Martin, R. L.; Morokuma, K.; Zakrzewski, V. G.; Voth, G. A.; Salvador, P.; Dannenberg, J. J.; Dapprich, S.; Daniels, A. D.; Farkas, Ö.; Foresman, J. B.; Ortiz, J. V.; Cioslowski, J.; Fox, D. J.; Gaussian 09, revision D.01, Gaussian, Inc., Wallingford, CT, 2010.

(65) Becke, A. D. Density-functional thermochemistry. III. The role of exact exchange. *J. Chem. Phys.* **1993**, *98*, 5648–5652.

(66) Perdew, J. P. Erratum: Density-functional approximation for the correlation energy of the inhomogeneous electron gas. *Phys. Rev. B* **1986**, *34*, 7406.

(67) Micera, G.; Garribba, E. The effect of the functional, basis set, and solvent in the simulation of the geometry and spectroscopic properties of $V^{IV}O^{2+}$ complexes. chemical and biological applications. *Int. J. Quantum Chem.* **2012**, *112*, 2486–2498.

(68) Bühl, M.; Reimann, C.; Pantazis, D. A.; Bredow, T.; Neese, F. Geometries of Third-Row Transition-Metal Complexes from Density-Functional Theory. *J. Chem. Theory Comput.* **2008**, *4*, 1449–1459.

(69) Marenich, A. V.; Cramer, C. J.; Truhlar, D. G. Universal solvation model based on solute electron density and on a continuum model of the solvent defined by the bulk dielectric constant and atomic surface tensions. *J. Phys. Chem. B* **2009**, *113*, 6378–6396.

(70) Neese, F. Software update: the ORCA program system, version 4.0. *Wiley Interdisciplinary Reviews: Computational Molecular Science* **2018**, *8*, e1327.

(71) Grimme, S. Semiempirical hybrid density functional with perturbative second-order correlation. *J. Chem. Phys.* **2006**, *124*, 34108.

(72) Micera, G.; Garribba, E. Is the spin-orbit coupling important in the prediction of the ^{51}V hyperfine coupling constants of $V^{IV}O^{2+}$ species? ORCA versus Gaussian performance and biological applications. *J. Comput. Chem.* **2011**, *32*, 2822–2835.

(73) Sanna, D.; Sciortino, G.; Ugone, V.; Micera, G.; Garribba, E. Nonoxido V(IV) Complexes: Prediction of the EPR Spectrum and Electronic Structure of Simple Coordination Compounds and Amavadin. *Inorg. Chem.* **2016**, *55*, 7373–7387.

(74) Casida, M. E. Time-dependent density-functional theory for molecules and molecular solids. *J. Mol. Struct. Theochem* **2009**, *914*, 3–18.

(75) Kundu, S.; Mondal, D.; Bhattacharya, K.; Endo, A.; Sanna, D.; Garribba, E.; Chaudhury, M. Nonoxido Vanadium(IV) Compounds Involving Dithiocarbazate-Based Tridentate ONS Ligands: Synthesis, Electronic and Molecular Structure, Spectroscopic and Redox Properties. *Inorg. Chem.* **2015**, *54*, 6203–6215.

(76) Allouche, A.-R. Gabedit—A graphical user interface for computational chemistry softwares. *J. Comput. Chem.* **2011**, *32*, 174–182.

(77) Jones, G.; Willett, P.; Glen, R. C.; Leach, A. R.; Taylor, R. Development and validation of a genetic algorithm for flexible docking. *J. Mol. Biol.* **1997**, *267*, 727–748.

(78) Sanna, D.; Ugone, V.; Sciortino, G.; Buglyó, P.; Bihari, Z.; Parajdi-Losonczi, P. L.; Garribba, E. $V^{IV}O$ complexes with antibacterial quinolone ligands and their interaction with serum proteins. *Dalton Trans.* **2018**, *47*, 2164–2182.

(79) Sciortino, G.; Sanna, D.; Ugone, V.; Maréchal, J.-D.; Garribba, E. Integrated ESI-MS/EPR/computational characterization of the binding of metal species to proteins: vanadium drug–myoglobin application. *Inorg. Chem. Front.* **2019**, *6*, 1561–1578.

(80) Ugone, V.; Sanna, D.; Sciortino, G.; Maréchal, J.-D.; Garribba, E. Interaction of Vanadium(IV) Species with Ubiquitin: A Combined Instrumental and Computational Approach. *Inorg. Chem.* **2019**, *58*, 8064–8078.

(81) Connolly, M. L. Analytical molecular surface calculation. *J. Appl. Crystallogr.* **1983**, *16*, 548–558.

(82) Lovell, S. C.; Word, J. M.; Richardson, J. S.; Richardson, D. C. The penultimate rotamer library. *Struct., Funct., Bioinf.* **2000**, *40*, 389–408.

(83) Machado, I.; Fernández, M.; Becco, L.; Garat, B.; Brissos, R. F.; Zabarska, N.; Gamez, P.; Marques, F.; Correia, I.; Pessoa, J. C.; Gambino, D. New metal complexes of NNO tridentate ligands: Effect of metal center and co-ligand on biological activity. *Inorg. Chim. Acta* **2014**, *420*, 39–46.

(84) Rodríguez-Hermida, S.; Wende, C.; Lago, A. B.; Carballo, R.; Kulak, N.; Vázquez-López, E. M. Reaction of a Bis(benzoylhydrazone) with Copper(II): Complex Formation, Hydroxylation, and DNA Cleavage Activity. *Eur. J. Inorg. Chem.* **2013**, *2013*, 5843–5853.

(85) Armstrong, C. M.; Bernhardt, P. V.; Chin, P.; Des Richardson, R. Structural Variations and Formation Constants of First-Row Transition Metal Complexes of Biologically Active Aroylhydrazones. *Eur. J. Inorg. Chem.* **2003**, *2003*, 1145–1156.

(86) Das, C.; Adak, P.; Mondal, S.; Sekiya, R.; Kuroda, R.; Gorelsky, S. I.; Chattopadhyay, S. K. Synthesis, Characterization, X-ray Crystal Structure, DFT Calculations, and Catalytic Properties of a Dioxidovanadium(V) Complex Derived from Oxamohydrazide and Pyridoxal: A Model Complex of Vanadate-Dependent Bromoperoxidase. *Inorg. Chem.* **2014**, *53*, 11426–11437.

(87) Mondal, S.; Das, C.; Ghosh, B.; Pakhira, B.; Blake, A. J.; Drew, M. G.B.; Chattopadhyay, S. K. Synthesis, spectroscopic studies, X-ray crystal structures, electrochemical properties and DFT calculations of three Ni(II) complexes of aroyl hydrazone ligands bearing anthracene moiety. *Polyhedron* **2014**, *80*, 272–281.

(88) Boas, L. V.; Pessoa, J. C. Vanadium, in: Comprehensive coordination chemistry. *ed. by Wilkinson, G.; Gillard, R. D.; McCleverty, J. A. Pergamon, Oxford* **1987**, *Vol. 3*, pp. 453–583.

(89) Fernández, M.; Becco, L.; Correia, I.; Benítez, J.; Piro, O. E.; Echeverria, G. A.; Medeiros, A.; Comini, M.; Lavaggi, M. L.; González, M. Oxidovanadium (IV) and dioxidovanadium (V) complexes of tridentate salicylaldehyde semicarbazones: searching for prospective antitrypanosomal agents. *J. Inorg. Biochem.* **2013**, *127*, 150–160.

(90) Di Marco, V. B.; Bombi, G. G. Electrospray mass spectrometry (ESI-MS) in the study of metal–ligand solution equilibria. *Mass Spectrom. Rev.* **2006**, *25*, 347–379.

(91) Sanna, D.; Ugone, V.; Micera, G.; Buglyó, P.; Bíró, L.; Garribba, E. Speciation in human blood of Metvan, a vanadium based potential anti-tumor drug. *Dalton Trans.* **2017**, *46*, 8950–8967.

(92) Sanna, D.; Ugone, V.; Sciortino, G.; Parker, B. F.; Zhang, Z.; Leggett, C. J.; Arnold, J.; Rao, L.; Garribba, E. $V^{IV}O$ and V^{IV} Species Formed in Aqueous Solution by the Tridentate Glutaroimide–Dioxime Ligand – An Instrumental and Computational Characterization. *Eur. J. Inorg. Chem.* **2018**, *2018*, 1805–1816.

(93) Sanna, D.; Varnágy, K.; Timári, S.; Micera, G.; Garribba, E. VO^{2+} Complexation by Bioligands Showing Keto–Enol Tautomerism: A Potentiometric, Spectroscopic, and Computational Study. *Inorg. Chem.* **2011**, *50*, 10328–10341.

(94) Karpishin, T. B.; Dewey, T. M.; Raymond, K. N. Coordination chemistry of microbial iron transport. 49. The vanadium(IV) enterobactin complex: structural, spectroscopic, and electrochemical characterization. *J. Am. Chem. Soc.* **1993**, *115*, 1842–1851.

(95) Maurya, M. R.; Uprety, B.; Avecilla, F.; Adão, P.; Pessoa, J. C. Vanadium (V) complexes of a tripodal ligand, their characterisation and biological implications. *Dalton Trans.* **2015**, *44*, 17736–17755.

(96) Adão, P.; Kuznetsov, M. L.; Barroso, S.; Martins, A. M.; Avecilla, F.; Pessoa, J. C. Amino alcohol-derived reduced Schiff base $V^{IV}O$ and V^{V} compounds as catalysts for asymmetric sulfoxidation of thioanisole with hydrogen peroxide. *Inorg. Chem.* **2012**, *51*, 11430–11449.

(97) Galloni, P.; Conte, V.; Floris, B. A journey into the electrochemistry of vanadium compounds. *Coord. Chem. Rev.* **2015**, *301-302*, 240–299.

(98) Hansch, C.; Leo, A. *Substituent constants for correlation analysis in chemistry and biology*; Wiley, 1979.

(99) Pisano, L.; Várnagy, K.; Timári, S.; Hegetschweiler, K.; Micera, G.; Garribba, E. $V^{IV}O$ Versus V^{IV} Complex Formation by Tridentate (O, Narom, O) Ligands: Prediction of Geometry, EPR ^{51}V Hyperfine Coupling Constants, and UV–Vis Spectra. *Inorg. Chem.* **2013**, *52*, 5260–5272.

(100) Sanna, D.; Várnagy, K.; Lihi, N.; Micera, G.; Garribba, E. Formation of New Non-oxido Vanadium(IV) Species in Aqueous Solution and in the Solid State by Tridentate (O, N, O) Ligands and Rationalization of Their EPR Behavior. *Inorg. Chem.* **2013**, *52*, 8202–8213.

(101) Morgenstern, B.; Kutzky, B.; Neis, C.; Stucky, S.; Hegetschweiler, K.; Garribba, E.; Micera, G. Synthesis and Characterization of Vanadium(IV) Complexes with cis-Inositol in Aqueous Solution and in the Solid-State. *Inorg. Chem.* **2007**, *46*, 3903–3915.

(102) Morgenstern, B.; Steinhauser, S.; Hegetschweiler, K.; Garribba, E.; Micera, G.; Sanna, D.; Nagy, L. Complex Formation of Vanadium(IV) with 1,3,5-Triamino-1,3,5-trideoxy-cis-inositol and Related Ligands. *Inorg. Chem.* **2004**, *43*, 3116–3126.

(103) Ribeiro, N.; Galvão, A. M.; Gomes, C. S. B.; Ramos, H.; Pinheiro, R.; Saraiva, L.; Ntungwe, E.; Isca, V.; Rijo, P.; Cavaco, I. Naphthoylhydrazones: coordination to metal ions and biological screening. *New J. Chem.* **2019**, *43*, 17801–17818.

(104) Maurya, M. R.; Khan, A. A.; Azam, A.; Ranjan, S.; Mondal, N.; Kumar, A.; Avecilla, F.; Pessoa, J. C. Vanadium complexes having $[V^{IV}O]^{2+}$ and $[V^{V}O_2]^{+}$ cores with binucleating dibasic tetradentate ligands: Synthesis, characterization, catalytic and antiamoebic activities. *Dalton Trans.* **2010**, *39*, 1345–1360.

(105) Santos, M. F. A.; Correia, I.; Oliveira, A. R.; Garribba, E.; Pessoa, J. C.; Santos-Silva, T. Vanadium Complexes as Prospective Therapeutics: Structural Characterization of a V^{IV} Lysozyme Adduct. *Eur. J. Inorg. Chem.* **2014**, *2014*, 3293–3297.

(106) Blagosklonny, M. V. Analysis of FDA Approved Anticancer Drugs Reveals the Future of Cancer Therapy. *Cell Cycle* **2004**, *3*, 1033–1040.

(107) Tai, S.; Sun, Y.; Squires, J. M.; Zhang, H.; Oh, W. K.; Liang, C.-Z.; Huang, J. PC3 is a cell line characteristic of prostatic small cell carcinoma. *The Prostate* **2011**, *71*, 1668–1679.

(108) da Silva, J. A. L.; da Silva, João JR Fraústo; Pombeiro, A. J. L. Amavadin, a vanadium natural complex: Its role and applications. *Coord. Chem. Rev.* **2013**, *257*, 2388–2400.

(109) Correia, I.; Adão, P.; Roy, S.; Wahba, M.; Matos, C.; Maurya, M. R.; Marques, F.; Pavan, F. R.; Leite, C. Q. F.; Avecilla, F.; Pessoa, J. C. Hydroxyquinoline derived vanadium(IV and V) and copper(II) complexes as potential anti-tuberculosis and anti-tumor agents. *J. Inorg. Biochem.* **2014**, *141*, 83–93.

(110) Correia, I.; Roy, S.; Matos, C. P.; Borovic, S.; Butenko, N.; Cavaco, I.; Marques, F.; Lorenzo, J.; Rodríguez, A.; Moreno, V.; Pessoa, J. C. Vanadium(IV) and copper(II) complexes of salicylaldimines and aromatic heterocycles: Cytotoxicity, DNA binding and DNA cleavage properties. *J. Inorg. Biochem.* **2015**, *147*, 134–146.

SYNOPSIS

Characterization and solution behavior of one oxidoethoxidovanadium(V) and two non-oxidovanadium(IV) complexes formed by three ONO donor aroylhydrazones are studied and their anti-proliferative activity and selectivity evaluated. In aqueous solution the complexes undergo partial change to $V^{V}O_2$ and $V^{IV}O$ complexes. Interactions of these $V^{V}O_2$, $V^{IV}O$ and V^{IV} species with proteins are investigated through docking approaches.

FOR TABLE OF CONTENTS ONLY